UC Berkeley

UC Berkeley Previously Published Works

Title

Anisotropic flow of identified hadrons in Xe-Xe collisions at sNN = 5.44 TeV

Permalink

https://escholarship.org/uc/item/53w9v9mx

Journal

Journal of High Energy Physics, 2021(10)

ISSN

1126-6708

Authors

Acharya, S
Adamová, D
Adler, A
et al.

Publication Date

2021-10-01

DOI

10.1007/jhep10(2021)152

Copyright Information

Peer reviewed

Anisotropic flow of identified hadrons in Xe-Xe collisions at $\sqrt{s_{\mathrm{NN}}} = 5.44\,\mathrm{TeV}$

The ALICE collaboration

E-mail: ALICE-publications@cern.ch

ABSTRACT: Measurements of elliptic (v_2) and triangular (v_3) flow coefficients of $\pi^\pm$, $K^\pm$, p+$\overline{\mathrm{p}}$, K_S^0, and $\Lambda+\overline{\Lambda}$ obtained with the scalar product method in Xe-Xe collisions at $\sqrt{s_{\mathrm{NN}}} = 5.44\,\mathrm{TeV}$ are presented. The results are obtained in the rapidity range $|y| < 0.5$ and reported as a function of transverse momentum, p_{T}, for several collision centrality classes. The flow coefficients exhibit a particle mass dependence for $p_{\mathrm{T}} < 3\,\mathrm{GeV}/c$, while a grouping according to particle type (i.e., meson and baryon) is found at intermediate transverse momenta ($3 < p_{\mathrm{T}} < 8\,\mathrm{GeV}/c$). The magnitude of the baryon v_2 is larger than that of mesons up to $p_{\mathrm{T}} = 6\,\mathrm{GeV}/c$. The centrality dependence of the shape evolution of the p_{T}-differential v_2 is studied for the various hadron species. The v_2 coefficients of $\pi^\pm$, $K^\pm$, and p+$\overline{\mathrm{p}}$ are reproduced by MUSIC hydrodynamic calculations coupled to a hadronic cascade model (UrQMD) for $p_{\mathrm{T}} < 1\,\mathrm{GeV}/c$. A comparison with v_{n} measurements in the corresponding centrality intervals in Pb-Pb collisions at $\sqrt{s_{\mathrm{NN}}} = 5.02\,\mathrm{TeV}$ yields an enhanced v_2 in central collisions and diminished value in semicentral collisions.

Contents

1 Introduction

Collisions of ultra-relativistic nuclei provide the opportunity to study in the laboratory the quark-gluon plasma (QGP), a state of deconfined quarks and gluons [1]. An important feature of the QGP is the collective expansion, called flow, due to pressure gradients in the geometrically overlapping matter in the collisions of nuclei. A direct experimental evidence of this collective flow is the observation of anisotropic flow [2], which arises from the asymmetry in the initial geometry of the collision combined with the initial state inhomogeneities of the system's energy density. Its magnitude is usually quantified by the harmonic coefficients v_n in a Fourier decomposition of the azimuthal distribution of particles with respect to the collision symmetry plane [3, 4]

$$\frac{\mathrm{d}N}{\mathrm{d}\varphi} \propto 1 + 2\sum_{n=1}^{\infty} v_n \cos[n(\varphi - \Psi_n)], \tag{1.1}$$

where φ is the azimuthal angle of the produced particle and Ψ_n is the n-th harmonic symmetry-plane angle in the collision. The second (v_2) and third (v_3) coefficients are called elliptic and triangular flow, respectively. While v_2 directly reflects the almond-shaped geometry of the interaction volume being the largest contribution to the asymmetry in non-central collisions, v_3 is generated by fluctuations in the initial distribution of nucleons in the overlap region [5–9]. For light and strange particles, both coefficients scale approximately linearly with the corresponding eccentricities ε_n $(v_n \approx \kappa_n \varepsilon_n)$ [10], which govern the shape of

the initial collision geometry. The coefficients κ_n are sensitive to the macroscopic properties of the QGP, such as the shear viscosity to entropy density ratio (η/s), and the lifetime of the system. A greater sensitivity to η/s is expected for higher-order flow coefficients [11, 12].

Measurements of anisotropic flow performed in Au-Au collisions at the Relativistic Heavy Ion Collider (RHIC) [13–16] and in Pb-Pb collisions at the Large Hadron Collider (LHC) [17–20] indicate that the QGP is strongly-coupled (i.e. constituents have small mean free path) and behaves like a nearly perfect fluid as the extracted η/s is close to the lower limit predicted by the anti-de Sitter/conformal field theory (AdS/CFT) correspondence of $1/(4\pi)$ (setting $\hbar = k_B = 1$) [21]. Recently, the v_n coefficients of unidentified charged particles have been measured in Xe-Xe collisions at the center-of-mass energy per nucleon pair $\sqrt{s_{NN}} = 5.44\,\mathrm{TeV}$ [22–24]. These measurements further constrain the transport coefficients of the medium, such as η/s and bulk viscosity to entropy density ratio (ζ/s), and initial state models. Furthermore, comparisons of the v_2 measurements in semicentral Xe-Xe collisions with those from Pb-Pb collisions in the same centrality intervals could provide direct information on the η/s. For these collisions, the two systems have similar ε_2 coefficients [25, 26] but different sizes, thus the influence of the initial state on η/s mostly cancels out in ratios of Xe-Xe/Pb-Pb v_2 and a finite η/s suppresses κ_2 by $1/R$, where R corresponds to the transverse size of the system [25]. Centrality estimates the degree of overlap between two colliding nuclei and is expressed as percentiles of the inelastic cross section, with low percentage values corresponding to the most central collisions. Stronger constraints can be placed by studying anisotropic flow of identified particles since the κ_n coefficients depend on particle mass, type, and kinematics [27]. In addition to probing η/s and ζ/s, the anisotropic flow of identified particles provides valuable information on the particle production mechanism in different transverse momentum, p_T, regions. For $p_T \lesssim 3\,\mathrm{GeV}/c$, the characteristic mass ordering (i.e., lighter particles having a larger v_n than that of heavier particles at fixed p_T), which arises from the interplay between radial flow (isotropic expansion) and anisotropic flow [28, 29], is described by hydrodynamic calculations [30–34]. This mass ordering provides constraints on both η/s and ζ/s as the magnitude of v_n depends on η/s, while the mass ordering is affected by ζ/s through its influence on radial flow. At intermediate p_T, $3 < p_T < 8\,\mathrm{GeV}/c$, a grouping of v_n of mesons and baryons is observed, with the flow of baryons being larger than that of mesons [32, 35–37]. While this supports the hypothesis of hadronization through quark coalescence (involving the combination of a quark and anti-quark to form a meson and three quarks to form a baryon) [38–40], alternate explanations are attempted in models in which particle production includes interactions of jet fragments with bulk matter [41]. To test the hypothesis of particle production via quark coalescence it was suggested to divide both v_n and p_T by the number of constituent quarks since it is assumed that the spectrum of produced particles is proportional to the product of the spectra of their constituents [42, 43]. However, deviations from the exact scaling at the level of $\pm 20\%$ are seen in Pb-Pb collisions at the LHC [30–32], while it only holds approximately at RHIC [37]. This scaling can be further tested using measurements of identified particle v_n in Xe-Xe collisions.

The p_T-differential elliptic flow coefficient, $v_2(p_T)$, of $\pi^\pm$, $K^\pm$, p+$\overline{\mathrm{p}}$, K_S^0, and $\Lambda + \overline{\Lambda}$ as well as the p_T-differential triangular flow coefficient, $v_3(p_T)$, of $\pi^\pm$, $K^\pm$, and p+$\overline{\mathrm{p}}$, measured

in Xe-Xe collisions at $\sqrt{s_{NN}} = 5.44$ TeV are presented in this paper. The results are reported for $p_T < 8.5$ GeV/c within the rapidity range $|y| < 0.5$ at different collision centralities in the 0–60% range, where v_n can be measured accurately. The scalar product method [44–46] is employed with a pseudorapidity gap of $|\Delta\eta| > 2.0$ between the identified particles under study and the reference charged particles. The v_n coefficients denote the average between results for positive and negative particles as they are compatible within uncertainties for most p_T and centrality intervals. Any residual difference has been included into the systematic uncertainties.

This paper is organized as follows. A brief description of the ALICE detector, analysis details, particle identification, reconstruction methods, and flow measurement techniques is given in section 2. Section 3 outlines the evaluation of systematic uncertainties, while the results are reported in section 4. Finally, conclusions are drawn in section 5.

2 Experimental setup and analysis details

A full overview of the ALICE detector and its performance can be found in refs. [47, 48]. The Inner Tracking System (ITS) [49], the Time Projection Chamber (TPC) [50], the Time of Flight (TOF) [51], and the V0 [52] are the main subsystems used in this analysis and are briefly described below. These detectors are located inside a solenoid magnet which provides a nominal magnetic field of 0.5 T. However, the field was reduced to 0.2 T for Xe-Xe collisions in order to extend particle tracking and identification to the lowest possible momenta. The ITS, TPC, and TOF detectors cover the full azimuth within the pseudorapidity range $|\eta| < 0.9$. The ITS consists of six layers of silicon detectors and is employed for tracking, vertex reconstruction, and event selection. The TPC, being the main tracking detector, is used to reconstruct charged-particle tracks but also to identify particles via the measurement of the specific energy loss, dE/dx. The TOF detector provides particle identification based on the measurement of flight time from the collision point using a start time given by the T0 detector [53], which consists of two arrays of Cherenkov counters located at $-3.3 < \eta < -3.0$ (T0C) and $4.5 < \eta < 4.9$ (T0A). The V0 detector, two arrays of 32 scintillator tiles each (four rings in the radial direction with each ring divided into eight sectors in the azimuthal direction) covering $-3.7 < \eta < -1.7$ (V0C) and $2.8 < \eta < 5.1$ (V0A), is used for triggering, event selection, and the determination of centrality [54] and $\mathbf{Q}_n$ vectors (see below). Two tungsten-quartz neutron Zero Degree Calorimeters (ZDCs) [55], installed 112.5 meters from the interaction point on each side, are also used for event selection.

The analyzed data set was recorded by the ALICE detector during the Xe-Xe run at $\sqrt{s_{NN}} = 5.44$ TeV in 2017. The minimum-bias trigger requires signals in both V0A and V0C detectors in coincidence with signals in the two neutron ZDCs, the latter condition suppressing contamination from electromagnetic interactions. In addition, the beam-induced background (i.e., beam-gas events) and pileup events are removed using an offline event selection. The former is rejected utilizing the V0 and ZDC timing information, while pileup events are removed by comparing charged particle multiplicity estimates from the V0 detector with those of tracking detectors at midrapidity, exploiting the difference in readout

times between the systems. The remaining contribution of such interactions is estimated to be negligible. The primary vertex position is determined from tracks reconstructed in the ITS and TPC as described in ref. [48]. Approximately 9×10^5 Xe-Xe events in the 0–60% centrality interval, with a primary vertex position within ± 10 cm from the nominal interaction point along the beam direction, are used in the analysis. Centrality is estimated from the energy deposition measured in the V0 detector [54].

The charged particle tracks used to determine the flow coefficients of $\pi^\pm$, $K^\pm$, and $p+\overline{p}$ are reconstructed using the ITS and TPC within $|\eta| < 0.8$ and $0.4 < p_T < 8.5 \, \text{GeV}/c$. Each track is required to cross at least 70 TPC readout rows (out of a maximum of 159), to have a minimum number of 70 TPC space points with a χ^2 per TPC space point lower than 4, and to have the ratio between the number of space points and the number of crossed rows in the TPC larger than 0.8. The selected tracks are also required to have at least 2 ITS hits, of which at least one in the two innermost layers, and a χ^2 per ITS hit smaller than 36. Only tracks with a distance of closest approach (DCA) to the reconstructed vertex position smaller than 2 cm in the longitudinal direction (z) are accepted. In the transverse plane (xy), a p_T-dependent selection is applied: $|\text{DCA}_{xy}| < 7\sigma_{\text{DCA}_{xy}}$, where $\sigma_{\text{DCA}_{xy}}$ is the resolution of the DCA_{xy} in each p_T interval. These selection criteria reduce the contamination from secondary charged particles (i.e., particles originating from weak decays, conversions, and secondary hadronic interactions in the detector material) and fake tracks (random associations of space points) and ensure a track momentum resolution better than 4% for the considered p_T range [56].

The particle identification for $\pi^\pm$, $K^\pm$, and $p+\overline{p}$ is performed using signals from the TPC and TOF detectors following the procedure described in ref. [32]. For $p_T < 4 \, \text{GeV}/c$, particle identification is done track-by-track evaluating the difference between the measured and expected dE/dx and time-of-flight for a given species in units of the standard deviation ($\sigma_{\text{TPC}}, \sigma_{\text{TOF}}$) from the most probable value. Particles are selected combining the TPC and TOF information ($n_{\sigma_{\text{PID}}} = \sqrt{n_{\sigma_{\text{TPC}}}^2 + n_{\sigma_{\text{TOF}}}^2}$) and requiring $n_{\sigma_{\text{PID}}} < 3$ for each species. When this condition is fulfilled by more than one species, the smallest $n_{\sigma_{\text{PID}}}$ is used to assign the identity. To exclude contamination in the sample from secondary protons originating from the detector material, only $\overline{p}$ are considered for $p_T < 2 \, \text{GeV}/c$. For $p_T > 4 \, \text{GeV}/c$, only $\pi^\pm$ and $p+\overline{p}$ are identified using the TPC dE/dx by selecting them from the upper part of the pion dE/dx distribution and from the lower part of the proton dE/dx distribution, respectively. For example, pion selection varies in the range 0.3σ to 2σ.

The remaining contamination from secondary particles originating in weak decays, studied using the procedure described in ref. [57], is negligible for $K^\pm$ and decreases with increasing p_T from about 5% to 0.5% for $\pi^\pm$ and from about 40% to 5% for $p+\overline{p}$ in the p_T range 0.4–4.0 GeV/c. The v_n coefficients are not corrected for these contaminations. Their effect on v_n, estimated from the correlation between v_n and contamination for various DCA_{xy} selections in each p_T interval, is negligible for $\pi^\pm$ and $K^\pm$ and up to 20% and 5% for central and peripheral collisions, respectively, for v_2 of $p+\overline{p}$ at $p_T \sim 0.5 \, \text{GeV}/c$. The contamination from other particle species is below 2% and 25% at $p_T > 4.0$ GeV/c for $\pi^\pm$ and $p+\overline{p}$, respectively. The contamination from fake tracks is negligible.

The K_S^0 and $\Lambda+\overline{\Lambda}$ are reconstructed in the $K_S^0 \to \pi^+ + \pi^-$ and $\Lambda \to p + \pi^-$ $(\overline{\Lambda} \to \overline{p} + \pi^+)$ channels. An offline selection is used to identify secondary vertices (called V^0s), from which two particles of opposite charge originate. The selection of V^0 candidates is done with an invariant mass between 0.4 and 0.6 GeV/c^2 for K_S^0 and 1.07 and 1.17 GeV/c^2 for $\Lambda+\overline{\Lambda}$. Daughter particles, identified using the TPC ($|n_{\sigma_{TPC}}| < 3$), are assumed to be either a π^+–π^- pair or a p–π^- ($\overline{p}$–π^+) pair in the calculation of the invariant mass of the V^0. The TPC track quality requirements described above for charged tracks are also imposed on daughter particles. In addition, the maximum DCA of daughter tracks to the secondary vertex is 0.5 cm and the minimum DCA of daughter tracks to the primary vertex is 0.1 cm. Secondary vertices created by decays into more than two particles are rejected requiring the cosine of the pointing angle θ_p to be larger than 0.998. This angle is defined as the angle between the momentum-vector of the V^0 assessed at its decay position and the line connecting the V^0 decay vertex to the primary vertex and has to be close to 0 as a result of momentum conservation. Only V^0 candidates produced at a radial distance between 5 and 100 cm from the beam line are accepted. Finally, a selection in the Armenteros-Podolanski variables [58] is applied for the K_S^0 candidates to asses the systematic uncertainty related to contamination from $\Lambda+\overline{\Lambda}$ and electron-positron pairs coming from γ conversions. Earlier studies have shown that contaminations from higher mass baryons ($\Xi^\pm$, $\Omega^\pm$) have a negligible effect on the measured v_n [30]. More details about this selection can be found in ref. [32].

The scalar product (SP) method [44–46] is used to measure the flow coefficients v_n, written as

$$v_n\{SP\} = \langle\langle \mathbf{u}_{n,k} \mathbf{Q}_n^* \rangle\rangle \Big/ \sqrt{\frac{\langle \mathbf{Q}_n \mathbf{Q}_n^{A*} \rangle \langle \mathbf{Q}_n \mathbf{Q}_n^{B*} \rangle}{\langle \mathbf{Q}_n^A \mathbf{Q}_n^{B*} \rangle}}, \qquad (2.1)$$

where $\mathbf{u}_{n,k} = \exp(in\varphi_k)$ is the unit flow vector of the particle of interest k with azimuthal angle φ_k, $\mathbf{Q}_n$ is the event flow vector, and n is the harmonic number. Brackets $\langle \cdots \rangle$ denote an average over all events, the double brackets $\langle\langle \cdots \rangle\rangle$ an average over all particles in all events, and $*$ the complex conjugate. The vector $\mathbf{Q}_n$ is obtained from the azimuthal distribution of the energy deposition measured in the V0A, with the x and y components given by

$$Q_{n,x} = \sum_j w_j \cos(n\varphi_j), \ Q_{n,y} = \sum_j w_j \sin(n\varphi_j), \qquad (2.2)$$

where the sum runs over the 32 channels j of the V0A detector, φ_j is the azimuthal angle of channel j, and w_j is the amplitude measured in channel j. The vectors $\mathbf{Q}_n^A$ and $\mathbf{Q}_n^B$ are determined from the azimuthal distribution of the energy deposition measured in the V0C and the azimuthal distribution of the tracks reconstructed in the ITS and TPC, respectively. Any non-uniform detector response is taken into account by adjusting the components of the $\mathbf{Q}_n$ vectors using a recentering procedure (i.e. subtraction of the $\mathbf{Q}_n$ vector averaged over many events from the $\mathbf{Q}_n$ vector of each event) [59]. The large gap in pseudorapidity between $\mathbf{u}_{n,k}$ and $\mathbf{Q}_n$ ($|\Delta\eta| > 2.0$) greatly suppresses short-range correlations unrelated to the common symmetry planes Ψ_n ("non-flow"), such as those due to resonances, jets, and quantum statistics correlations. The remaining non-flow contributions are small as reported in ref. [22] where the ratio between $v_2\{4\}$ and $v_2\{2, |\Delta\eta| > 2.0\}$ of inclusive charged
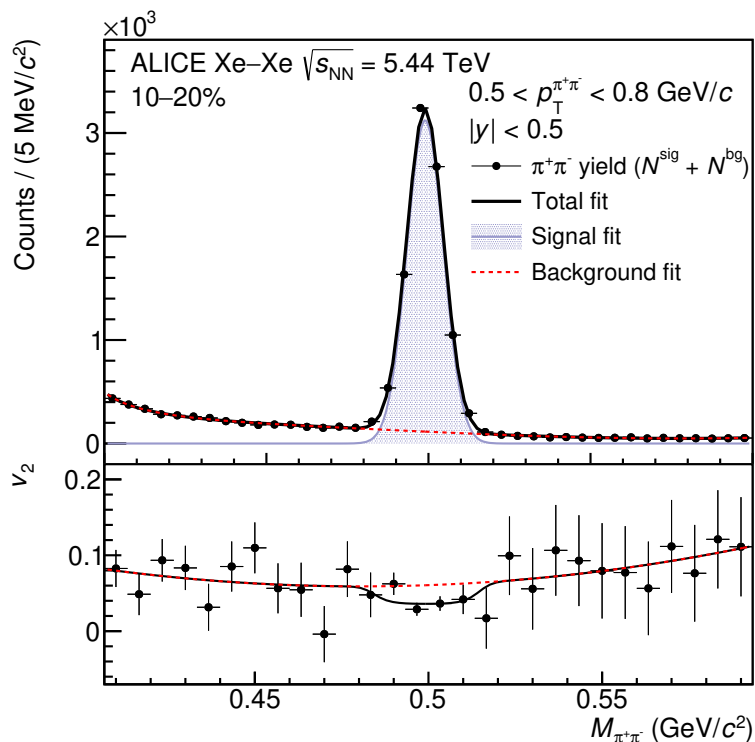
Figure 1. Top panel: invariant mass distribution of opposite-sign pion pairs belonging to candidate K_S^0 in the centrality range 10–20% and p_T interval $0.5 < p_T^{\pi^+\pi^-} < 0.8 \, \text{GeV}/c$. Bottom panel: a fit of eq. (2.3) to the mass-dependent v_2 distribution.

particles shows a weak centrality dependence for semicentral and peripheral collisions. These contributions are estimated by increasing the pseudorapidity gap to $|\Delta\eta| > 2.8$. Any residual difference has been included into the systematic uncertainties (see section 3).

As the V^0s cannot be identified on a track-by-track basis, eq. (2.1) cannot be used to measure directly v_n of K_S^0 and $\Lambda+\overline{\Lambda}$. Instead, a statistical approach is employed, with the v_n^{tot} of the candidate V^0s being written as the weighted sum of $v_n(p_T)$ of the true V^0s, v_n^{sig}, and that of the background pairs, v_n^{bg} [60]

$$v_n^{\text{tot}}(M_{\text{d}^+\text{d}^-}) = v_n^{\text{sig}} \frac{N^{\text{sig}}}{N^{\text{sig}} + N^{\text{bg}}}(M_{\text{d}^+\text{d}^-}) + v_n^{\text{bg}}(M_{\text{d}^+\text{d}^-}) \frac{N^{\text{bg}}}{N^{\text{sig}} + N^{\text{bg}}}(M_{\text{d}^+\text{d}^-}), \qquad (2.3)$$

where signal (N^{sig}) and background (N^{bg}) yields are extracted by integration of the Gaussian distribution and the third-order polynomial function used to parametrize the invariant mass ($M_{\text{d}^+\text{d}^-}$) distribution at the given p_T, respectively. The latter accounts for residual contaminations that are present in the K_S^0 and $\Lambda+\overline{\Lambda}$ signals after passing the selection criteria. The $v_n^{\text{tot}}(M_{\text{d}^+\text{d}^-})$ obtained according to eq. (2.1) is fitted using eq. (2.3) with one parameter for the v_n^{sig} and a second-order polynomial function to parametrize the v_n^{bg}. This procedure is illustrated in figure 1 where the invariant mass distribution of the K_S^0 and a fit of the $v_2^{\text{tot}}(M_{\pi^+\pi^-})$ distribution are shown in the top and bottom panels, respectively.

The $\pi^\pm$ and $p+\overline{p}$ v_2 and v_3 are reported for $0.4 < p_T < 8.5 \, \text{GeV}/c$ and $0.4 < p_T < 6.0 \, \text{GeV}/c$, respectively, while $K^\pm$ v_n are presented for $0.4 < p_T < 4.0 \, \text{GeV}/c$. The v_2 of K_S^0 and $\Lambda+\overline{\Lambda}$ are

reported for $0.5 < p_T < 6.0\,\mathrm{GeV}/c$ and $0.8 < p_T < 6.0\,\mathrm{GeV}/c$, respectively. All measurements are performed in the rapidity range $|y| < 0.5$.

3 Systematic uncertainties

The systematic uncertainties are evaluated by varying the event and charged particle tracking selection criteria, the particle identification approach, the V^0 finding strategy, and the $v_n(p_T)$ extraction. The default result is compared to a variation on the nominal measurement. If the value of the variation itself differs from the main result by more than 1σ, which is evaluated based on the recommendations in ref. [61], it is considered to be a systematic uncertainty. For various checks performed to quantify the effect of one systematic uncertainty (e.g., using different values for the minimum number of TPC space points employed in the reconstruction to estimate an uncertainty in tracking), the maximum significant deviation found between the nominal measurement and the systematic variations is assigned as a systematic uncertainty. The total systematic uncertainties are estimated by summing in quadrature the systematic uncertainties from the independent sources (if applicable) for all particle species, $v_n(p_T)$, and centrality intervals. A p_T-dependent systematic uncertainty is assigned to v_n of $\pi^\pm$, $K^\pm$, and p+$\overline{p}$, while a p_T-independent average uncertainty is reported for v_2 of K^0_S and $\Lambda+\overline{\Lambda}$. For each particle species, a summary of the magnitude of the relative systematic uncertainties on the values of v_2 and v_3 are given in tables 1 and 2, respectively.

Systematic uncertainties related to event selection criteria are estimated by using an alternative centrality estimator based either on the number of hits in the first or second layer of the ITS; by requiring the reconstructed primary vertex position alternatively within ± 12 cm, ± 7 cm, and ± 5 cm from the nominal interaction point along the beam direction; by imposing a stricter pileup rejection than the default selection (i.e., stronger constraints on the consistency of different event multiplicity estimators) or accepting all events with tracks regardless the pileup selection. The limited size of the Xe-Xe data sample does not allow for testing the effects from centrality fluctuations by measuring the v_n of $\pi^\pm$, $K^\pm$, and p+$\overline{p}$ in 1% wide centrality intervals as done in refs. [22, 32]. However, the systematic uncertainties estimated for this check in the v_n analysis of unidentified charged particles [22] are applied to the ones for v_n of $\pi^\pm$, $K^\pm$, and p+$\overline{p}$.

The variations for the track selection criteria are: changing the ITS hit requirements (referred to as tracking mode in tables 1 and 2); varying the minimum number of TPC space points from 70 to 60, 80, and 90; changing the χ^2 per ITS hit; increasing the minimum number of crossed TPC readout rows from 70 to 120 and the ratio between the number of space points and the number of crossed rows in the TPC from 0.8 to 0.9 (these two checks are combined and referred to as track quality in tables 1 and 2).

The uncertainties related to particle identification are evaluated by changing the required minimum number of TPC clusters from 70 to 60, 80, and 90 to estimate the effect on the dE/dx; varying the maximum value of the n_{σ_PID} from 3 to 1, 2, and 4 for $p_T < 4\,\mathrm{GeV}/c$; rejecting tracks that satisfy the particle identification criterion for more than one particle species simultaneously for $p_T < 4\,\mathrm{GeV}/c$; changing the n_{σ_TPC} ranges for $p_T > 4\,\mathrm{GeV}/c$.

Uncertainty source	$\pi^{\pm}$	$K^{\pm}$	$p+\overline{p}$	K_S^0	$\Lambda+\overline{\Lambda}$
Vertex position	0–3%	0–2%	1–3%	1–2%	1–2%
1% wide centrality intervals	0–2%	0–2%	0–2%		
Centrality estimator	0–4%	0–2%	1–4%	2–3%	1–3%
Pileup rejection	0–1%	0–1%	0–1%	0–1%	0–1%
Tracking mode	0–2%	0–3%	0–5%		
Number of TPC space points	0–1%	0–2%	0–3%	0–1%	0–1%
Track quality	0–1%	0–1%	0–1%	0–2%	1–2%
ITS χ^2	*negl.*	0–1%	0–1%		
Particle identification purity	1–2%	1–2%	1–3%	1–3%	1–2%
Number of TPC clusters used for dE/dx	0–1%	0–1%	0–1%	1–3%	1–3%
Exclusive particle identification	*negl.*	*negl.*	*negl.*		
Decay vertex (radial position)				1–2%	1–4%
Armenteros-Podolanski variables				1–2%	
DCA decay products to primary vertex				0–2%	1–2%
DCA between decay products				1–2%	1–2%
Pointing angle cos θ_p				0–1%	*negl.*
Minimum p_T of daughter tracks				1–2%	0–1%
dE/dx contamination for K_S^0				0–2%	
V^0 online selection				1–3%	0–2%
Peak shape				0–1%	0–1%
Residual background in yield				1–2%	0–1%
Positive and negative rapidities	1–2%	1–2%	1–3%	2–3%	1–3%
Opposite charges	0–2%	0–2%	0–2%		
v_n^{bg} parametrization				0–1%	1–2%
v_n^{tot} fit ranges				0–1%	0–2%

Table 1. Summary of systematic uncertainties for the v_2 of $\pi^{\pm}$, $K^{\pm}$, $p+\overline{p}$, K_S^0, and $\Lambda+\overline{\Lambda}$. Uncertainties are given as intervals between the minimum and maximum values for all p_T and centrality ranges. Empty fields indicate that a given check does not apply, while the field marked *negl.* for negligible implies that the tested uncertainty cannot be resolved within the statistical precision.

The systematic uncertainty related to the V^0 finding strategy includes contributions from the topological selection criteria on the V^0s themselves and requirements imposed on their daughter tracks. The latter consists of the following variations: requiring in addition $p_T > 0.2$ GeV/c for each daughter track; changing the minimum number of TPC space points from 70 to 60 and 80; varying the minimum number of crossed TPC readout rows from 70 to 60 and 80; increasing the ratio between the number of space points and the

Uncertainty source	$\pi^\pm$	$K^\pm$	$p+\overline{p}$
Vertex position	1–3%	1–2%	1–3%
1% wide centrality intervals	0–2%	0–2%	0–2%
Centrality estimator	2–4%	1–3%	2–4%
Pileup rejection	0–1%	0–1%	0–1%
Tracking mode	0–2%	0–4%	0–4%
Number of TPC space points	0–1%	0–3%	0–2%
Track quality	0–1%	0–1%	0–1%
ITS χ^2	0–1%	0–1%	0–1%
Particle identification purity	1–3%	1–2%	2–3%
Number of TPC clusters used for $\mathrm{d}E/\mathrm{d}x$	0–2%	0–1%	0–2%
Exclusive particle identification	*negl.*	*negl.*	*negl.*
Positive and negative rapidities	1–3%	1–2%	1–3%
Opposite charges	0–2%	0–2%	0–2%

Table 2. Summary of systematic uncertainties for the v_3 of $\pi^\pm$, $K^\pm$, and $p+\overline{p}$. Uncertainties are given as intervals between the minimum and maximum values for all p_T and centrality ranges. The field marked *negl.* for negligible implies that the tested uncertainty cannot be resolved within the statistical precision.

number of crossed rows in the TPC from 0.8 to 0.9; varying the minimum DCA of the V^0 daughter tracks to the primary vertex from 0.1 cm to 0.05 cm and 0.3 cm; changing the maximum DCA of the V^0 daughter tracks to the secondary vertex from 0.5 cm to 0.3 cm and 0.7 cm; requesting at least 60 and 90 TPC clusters instead of 70 to estimate the effect on the $\mathrm{d}E/\mathrm{d}x$; varying the maximum absolute value of the n_{σ_TPC} from 3 to 1 and 4. Concerning the V^0s selection, the following variations are investigated: changing the minimum value of the $\cos\theta_\mathrm{p}$ from 0.998 to 0.98; requesting a minimum radial distance to the beam line at which the V^0 can be produced of 1 cm and 15 cm instead of 5 cm; changing the maximum radial distance to the beam pipe at which the V^0 can be produced from 100 cm to 50 cm and 150 cm; suppressing the contamination from $\Lambda+\overline{\Lambda}$ and electron-positron pairs coming from γ conversions to the K^0_S sample by limiting the value of the Armenteros-Podolanski variables and excluding electrons by only selecting V^0 daughter tracks with a $\mathrm{d}E/\mathrm{d}x$ value 2σ away from the expected electron $\mathrm{d}E/\mathrm{d}x$. Finally, the yield extraction is varied by using polynomials of different orders as parametrization of the residual background in the invariant mass spectra and employing a sum of two Gaussian distributions with the same mean for the parametrization of the K^0_S and $\Lambda+\overline{\Lambda}$ invariant mass yield.

The uncertainties associated with the determination of $v_\mathrm{n}(p_\mathrm{T})$ are estimated by performing the analysis for positive and negative rapidities independently, thus increasing the pseudorapidity gap to $|\Delta\eta| > 2.8$; performing the analysis for $\pi^\pm$, $K^\pm$, and $p+\overline{p}$ for positive and negative charges independently; varying the $M_{\mathrm{d}^+\mathrm{d}^-}$ range over which eq. (2.3) is fitted; changing the v_2^bg parametrization from a second-order polynomial to a linear or constant function.
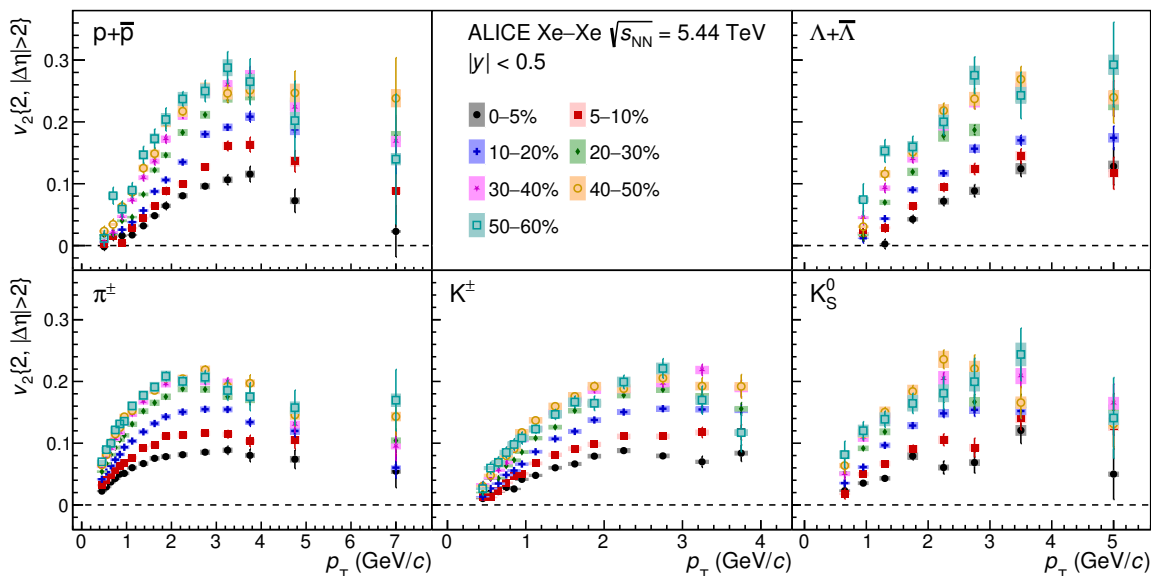
Figure 2. Centrality dependence of $v_2(p_T)$ for $\pi^{\pm}$, $K^{\pm}$, p+$\overline{\text{p}}$, K_S^0, and $\Lambda+\overline{\Lambda}$. Bars (boxes) denote statistical (systematic) uncertainties.

4 Results and discussion

4.1 Centrality and p_T dependence of flow coefficients

The $v_2(p_T)$ of $\pi^{\pm}$, $K^{\pm}$, p+$\overline{\text{p}}$, K_S^0, and $\Lambda+\overline{\Lambda}$ is presented in figure 2 for various centrality intervals in the 0–60% range. The measured v_2 of all particle species, being mainly driven by the collision geometry, increases strongly with decreasing centrality up to the 40–50% centrality interval. This evolution is expected since v_2 scales approximately linearly with the eccentricity of the overlap zone of the colliding nuclei [10]. For the 50–60% centrality class, the value of v_2 is similar to that measured in the previous centrality interval within uncertainties, which is expected due to a shorter lifetime of the system in more peripheral collisions. This together with the reduced contribution of eccentricity fluctuations and hadronic interactions inhibit the generation of large v_2 [62, 63]. The $v_2(p_T)$ increases up to $p_T \sim 3$–4 GeV/c, where a maximum is reached, and then decreases with increasing p_T. The position of this maximum depends weakly on centrality and is located at smaller p_T for lighter compared to heavier particles, over the various centrality intervals studied. The observed phenomenon finds an explanation in the changes in parton density and the centrality dependence of radial flow [32], which will be detailed in section 4.3. The evolution of v_2 with p_T and centrality is similar to that reported in Pb-Pb collisions [30–32].

Unlike v_2, the third-order flow coefficient v_3 originates from event-by-event fluctuations in the initial nucleon density distribution [5–9]. A stronger decrease of v_3 compared to v_2 is expected due to the dampening effect of η/s, which implies that v_3 is more sensitive to transport coefficients than v_2 [11, 12]. The limited size of the Xe-Xe data sample does not allow for v_3 to be measured accurately in the centrality intervals used for v_2. Therefore, these measurements have been combined in larger centrality classes using the p_T-differential
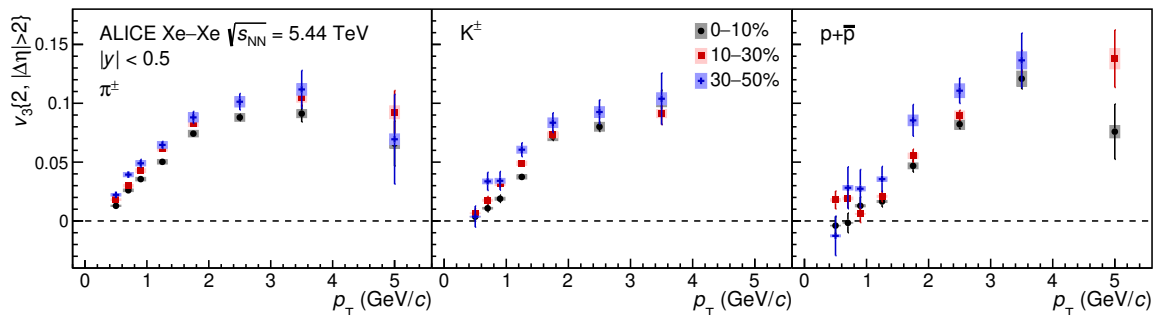
Figure 3. Centrality dependence of $v_3(p_T)$ for $\pi^{\pm}$, $K^{\pm}$, and p+$\overline{\text{p}}$. Bars (boxes) denote statistical (systematic) uncertainties.

yields [64] as weights. Figure 3 presents the $v_3(p_T)$ of $\pi^{\pm}$, $K^{\pm}$, and p+$\overline{\text{p}}$ for the 0–10%, 10–30%, and 30–50% centrality intervals. The measured v_3 is non-zero, positive for most of the p_T ranges and increases with p_T up to 3–4 GeV/c. The coefficient v_3 shows a weak centrality dependence with a magnitude significantly smaller than that of v_2, except for the 0–10% centrality interval. These findings illustrate that v_3 originates from fluctuations of the initial geometry of the system.

Figure 4 shows comparisons of the $v_2(p_T)$ for all particle species in a given centrality interval arranged into panels of various centrality classes. For $p_T < 2$–3 GeV/c, v_2 of the different particle species exhibits a mass ordering, meaning that heavier particles have a smaller v_2 than that of lighter particles at the same p_T. This behaviour can be attributed to the interplay of elliptic flow with radial flow which imposes an isotropic velocity boost equal for all particles, thus pushing heavier particles towards higher p_T [28, 29]. For $3 < p_T < 8$ GeV/c, the v_2 of baryons becomes larger than that of mesons, indicating that the particle type dependence persists out to high p_T. This grouping according to the number of constituent quarks supports the hypothesis of particle production via quark coalescence [38]. The crossing between meson and baryon v_2 depends on particle species and centrality, occurring at lower p_T values for peripheral than central collisions as a result of the smaller radial flow in the former. Comparing the $K^{\pm}$ and K_S^0 v_2, there is a hint of $v_2^{K_S^0} < v_2^{K^{\pm}}$ in the 0–10% centrality range, while the measurements are compatible within statistical uncertainties in the 10–60% centrality interval. One should note that a difference in $v_2(p_T)$ of $K^{\pm}$ and K_S^0 was reported by ALICE in Pb-Pb collisions [30, 32].

Figure 5 presents the $v_3(p_T)$ of $\pi^{\pm}$, $K^{\pm}$, and p+$\overline{\text{p}}$ in a given centrality interval. The v_3 of different particle species is mass ordered at $p_T < 2$–3 GeV/c, indicating the interplay between triangular and radial flow. For $3 < p_T < 6$ GeV/c, the p+$\overline{\text{p}}$ v_3 is slightly larger than that of $\pi^{\pm}$. The crossing between v_3 values of pions and protons shows a weak centrality dependence.

4.2 Scaling properties

Scaling with the number of constituent quarks (NCQ) of v_n has been suggested to test the hypothesis of particle production via quark coalescence at intermediate p_T, which would lead to a meson and baryon v_n grouping [38–40]. This can be achieved by dividing both v_n
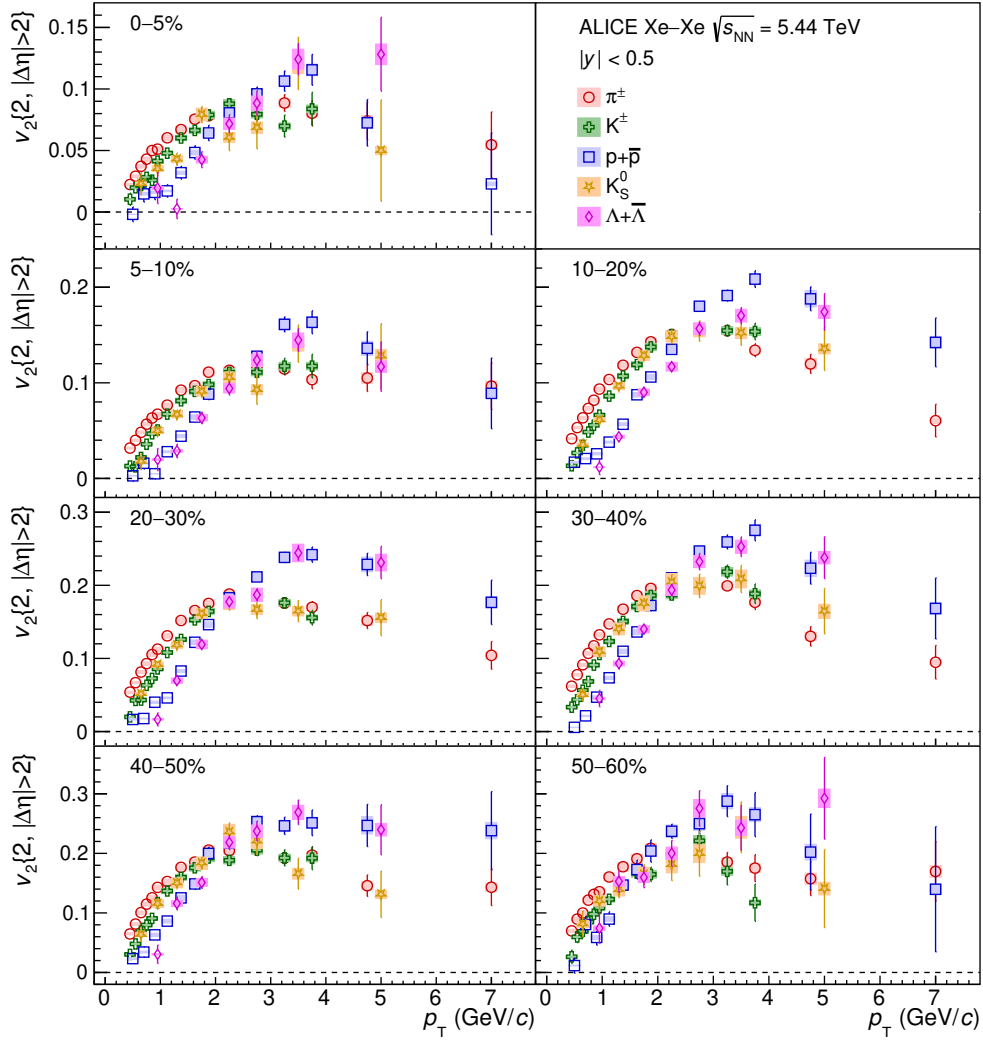
Figure 4. The p_T-differential v_2 of $\pi^\pm$, $K^\pm$, p+$\overline{p}$, K^0_S, and $\Lambda+\overline{\Lambda}$ in a given centrality interval. Bars (boxes) denote statistical (systematic) uncertainties.
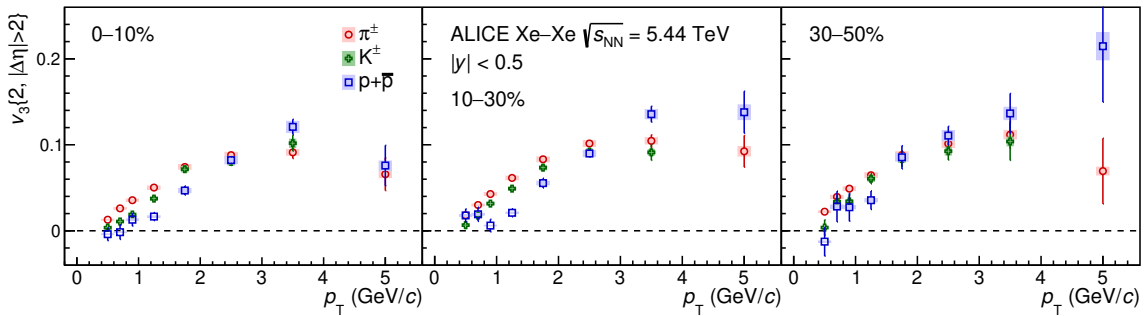

Figure 5. The p_T-differential v_3 of $\pi^\pm$, $K^\pm$, and p+$\overline{p}$ in a given centrality interval. Bars (boxes) denote statistical (systematic) uncertainties.
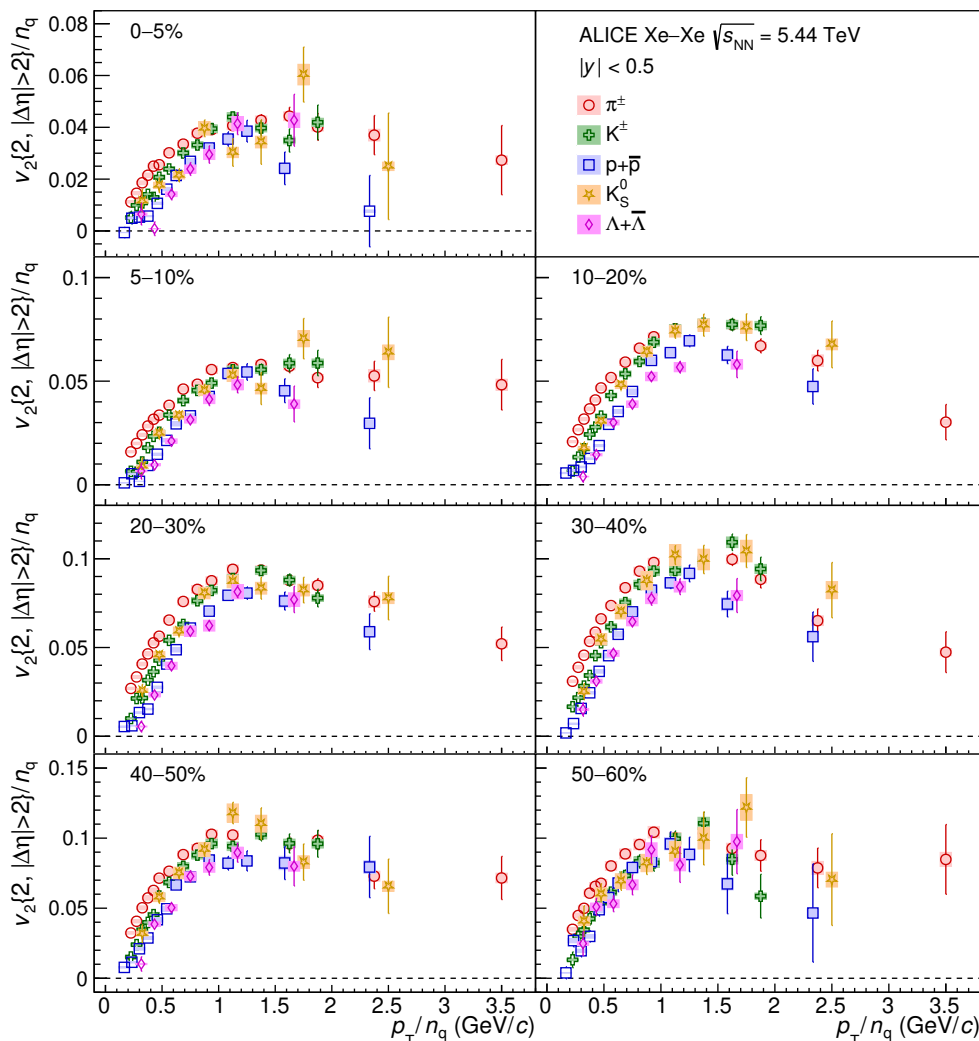
Figure 6. The p_T/n_q dependence of v_2/n_q of $\pi^\pm$, $K^\pm$, $p+\overline{p}$, K^0_S, and $\Lambda+\overline{\Lambda}$ for various centrality classes. Bars (boxes) denote statistical (systematic) uncertainties.

and p_T by the number of constituent quarks (n_q) independently for each particle species. Figures 6 and 7 present the v_2/n_q and v_3/n_q as function of p_T/n_q for $\pi^\pm$, $K^\pm$, $p+\overline{p}$, K^0_S, and $\Lambda+\overline{\Lambda}$, for various centrality classes. For $1 < p_T/n_q < 3\,\text{GeV}/c$, the region where quark coalescence is hypothesized to be the dominant process [38, 39], a deviation from the exact scaling of $\pm\,20\%$ is found for v_2, similar to the one reported in Pb-Pb collisions [30–32]. This deviation is quantified by dividing the p_T/n_q dependence of v_2/n_q by a cubic spline fit to the $p+\overline{p}$ v_2/n_q. The scaling for v_3 seems to hold within the relatively large uncertainties.

4.3 Shape evolution of $v_2(p_T)$ as function of centrality

The centrality dependence of the shape evolution of $v_2(p_T)$ is studied as in ref. [32] by choosing the v_2 measured in the 20–30% centrality interval as reference. It is quantified by dividing the $v_2(p_T)$ in a given centrality interval by this reference and denoted as $v_2(p_T)_{\text{ratio to }20–30\%}$ in the following. The ratio of the p_T-integrated v_2 value obtained in
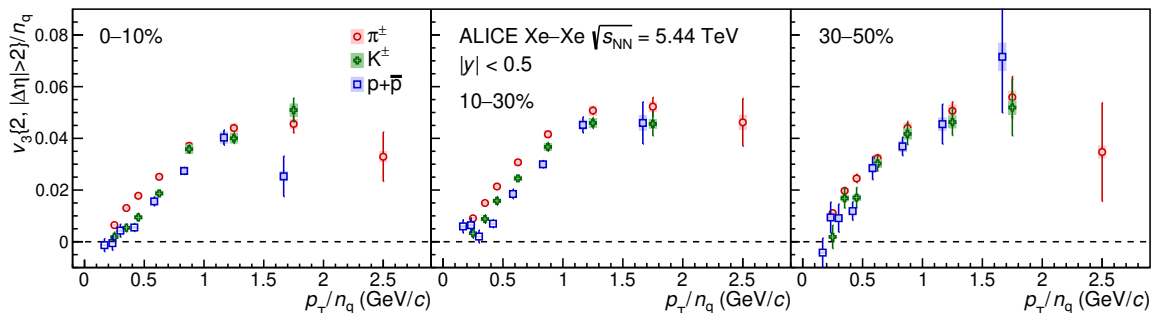
Figure 7. The p_T/n_q dependence of v_3/n_q of $\pi^\pm$, $K^\pm$, and p+$\overline{\text{p}}$ for various centrality classes. Bars (boxes) denote statistical (systematic) uncertainties.

the 20–30% centrality interval to that in the centrality interval of interest is used as a normalization factor in order for $v_2(p_T)_{\text{ratio to 20–30\%}}$ to be unity in the absence of centrality-dependent variations. The shape evolution of elliptic flow for $\pi^\pm$, $K^\pm$, p+$\overline{\text{p}}$, and inclusive charged hadrons (the latter taken from ref. [22]) is presented in figure 8. Variations in shape of about 10% are observed for inclusive charged hadrons throughout the considered p_T range within uncertainties. The evolution of the shape of the $v_2(p_T)$ shows different trends for $\pi^\pm$, $K^\pm$, and p+$\overline{\text{p}}$ for $p_T < 2$ GeV/c and no particle type dependence within uncertainties for $p_T \geq 2$ GeV/c. The variations are more pronounced for p+$\overline{\text{p}}$ $v_2(p_T)_{\text{ratio to 20–30\%}}$, reaching around 60% at low p_T in peripheral collisions. The elliptic flow of $K^\pm$ varies up to 40% for $p_T < 1$ GeV/c, while the $v_2(p_T)_{\text{ratio to 20–30\%}}$ of $\pi^\pm$ follows the results for inclusive charged particles. Radial flow and transverse quark density should play important roles in this mass dependence for $p_T < 2$ GeV/c as both depend on centrality, having larger values in central than peripheral collisions. The latter influences the peak value of $v_n(p_T)$ in the coalescence model [65], while the effect of the former on v_n of heavier particles is greater than on the lighter particles at low p_T.

An alternative way of quantifying the shape of the $v_2(p_T)$ is the position of the maximum v_2. It is expected to be located at higher p_T in central than peripheral collisions as the quark density depends on centrality. Its centrality dependence, quantified by the p_T where $v_2(p_T)$ reaches a maximum divided by the number of constituent quarks n_q, is reported in figure 9 for $\pi^\pm$ and p+$\overline{\text{p}}$. The $K^\pm$, K^0_S, and $\Lambda+\overline{\Lambda}$ are not included since the kinematic range and granularity of the measurements do not allow for a reliable extraction of a maximum. The p_T/n_q at which $v_2(p_T)$ reaches a maximum, denoted as $p_T|_{v_2^{\max}}$, shows a weak centrality dependence with a decreasing trend from central to peripheral collisions. This behavior is expected from the hypothesis of hadronization through coalescence where an increase in the transverse density of quarks, as in more central collisions, results in a higher value of $p_T|_{v_2^{\max}}$ [65]. The observed $p_T|_{v_2^{\max}}$ is compatible between $\pi^\pm$ and p+$\overline{\text{p}}$ for all centrality intervals within uncertainties. The systematic uncertainties presented in figure 9 are evaluated directly on $p_T|_{v_2^{\max}}$ to accurately take into account that some systematic uncertainties can be point-by-point correlated in p_T.

If v_2 exhibits a power law dependence on p_T^2 up to $p_T \sim M$ for particles with mass M as in the scenario of ideal hydrodynamics [66], ratios of the form $|v_2|^{1/2}/p_T$ should
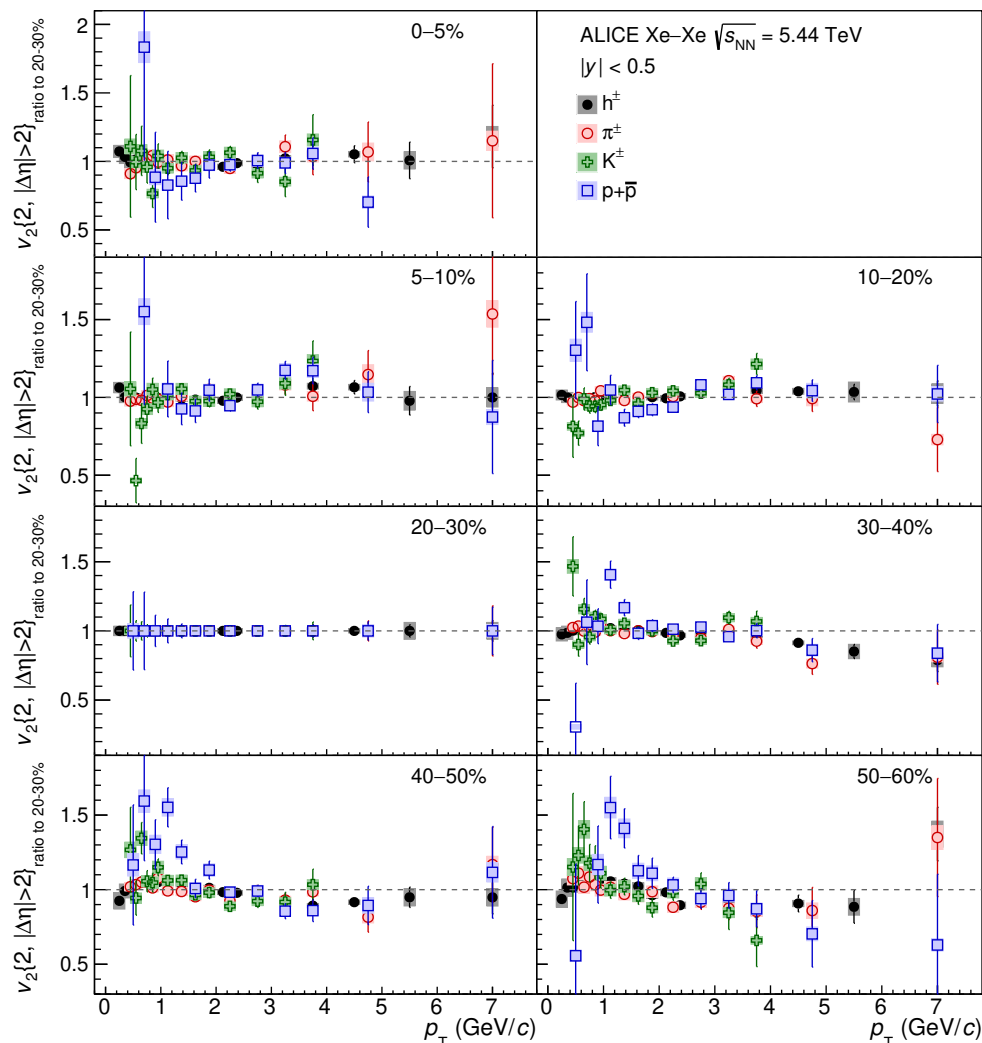
Figure 8. Centrality dependence of $v_2(p_T)_{\text{ratio to } 20-30\%}$ for $\pi^\pm$, $K^\pm$, $p+\bar{p}$, and inclusive charged hadrons ($h^\pm$) [22]. Bars (boxes) denote statistical (systematic) uncertainties.

be constant. Previous measurements performed by ALICE in Pb-Pb collisions [32] have shown that the $v_2 \propto p_T{}^2$ scaling is broken for $\pi^\pm$ and the inclusive charged particles for all centrality intervals. However, this scaling holds up to $p_T \approx 1\,\text{GeV}/c$ for $K^\pm$ and K^0_S, and up to $p_T \approx 2\,\text{GeV}/c$ for $p+\bar{p}$ and $\Lambda+\overline{\Lambda}$ for central and semicentral collisions [32]. It should be noted, however, that the kinematic constraints imposed on the measurement preclude testing the scaling hypothesis in the full relevant momentum region for $\pi^\pm$ and the inclusive charged particles. Figure 10 shows $|v_2|^{1/2}/p_T$ for inclusive charged particles [22], $\pi^\pm$, $K^\pm$, $p+\bar{p}$, K^0_S, and $\Lambda+\overline{\Lambda}$ as a function of p_T in various centrality intervals. The ratios $|v_2|^{1/2}/p_T$ show a strong p_T dependence for $\pi^\pm$ and the inclusive charged particles, while they exhibit a weak (if any) p_T dependence up to $p_T \approx 1\,\text{GeV}/c$ for $K^\pm$ and K^0_S, and up to $p_T \approx 2\,\text{GeV}/c$ for $p+\bar{p}$ and $\Lambda+\overline{\Lambda}$ for the 0–5% and 10–20% centrality intervals.
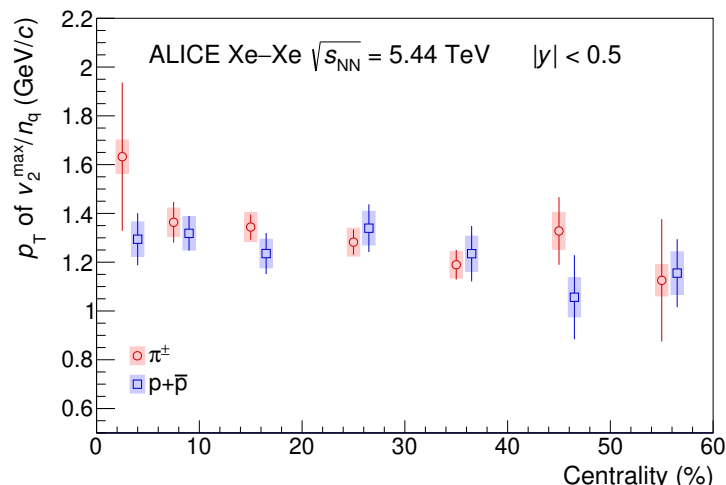
Figure 9. Centrality dependence of $p_\mathrm{T}|_{v_2^{\mathrm{max}}}$ for $\pi^\pm$ and p+$\overline{\mathrm{p}}$ divided by number of constituent quarks, n_q. The p+$\overline{\mathrm{p}}$ points are slightly shifted along the horizontal axis for better visibility. Bars (boxes) denote statistical (systematic) uncertainties.
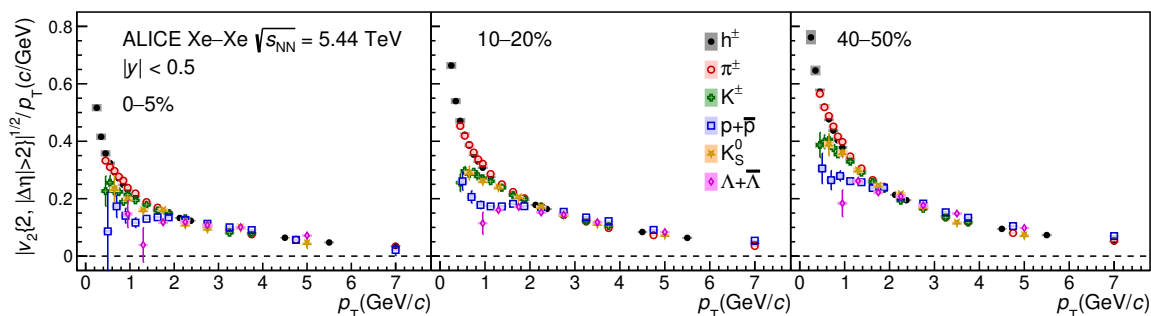
Figure 10. $|v_2|^{1/2}/p_\mathrm{T}$ of inclusive charged hadrons (h$^\pm$) [22], $\pi^\pm$, K$^\pm$, p+$\overline{\mathrm{p}}$, K$_\mathrm{S}^0$, and $\Lambda+\overline{\Lambda}$ as function of p_T for various centrality intervals. Bars (boxes) denote statistical (systematic) uncertainties.

4.4 Comparison with hydrodynamic calculations

Figure 11 presents the p_T-differential v_2 of $\pi^\pm$, K$^\pm$, and p+$\overline{\mathrm{p}}$ for various centrality intervals compared with predictions from MUSIC hydrodynamic simulations [67]. MUSIC [68], an event-by-event 3+1 dimensional viscous hydrodynamic model, uses the IP-Glasma model [69, 70] to describe the initial conditions of the collision and is coupled to a hadronic cascade model (UrQMD) [71, 72], which allows one to study the influence of the hadronic phase on the development of anisotropic flow for different particle species. The starting time for the hydrodynamic evolution and the switching energy between hydrodynamics and the microscopic transport evolution are set to $\tau_0 = 0.4\,\mathrm{fm}/c$ and $e_\mathrm{sw} = 0.18\,\mathrm{GeV/fm}^3$, respectively. A value of $\eta/s = 0.12$ and a temperature dependent ζ/s are also employed in this model. It should be noted that these parameters do not depend on collision system or centrality.

Figure 11 shows that the MUSIC calculations qualitatively reproduce the mass ordering. The predictions are in agreement with the measured $v_2(p_\mathrm{T})$ of $\pi^\pm$, K$^\pm$, and p+$\overline{\mathrm{p}}$ for $p_\mathrm{T} < 1\,\mathrm{GeV}/c$, while they overestimate the data points at higher p_T. However, the v_2 of
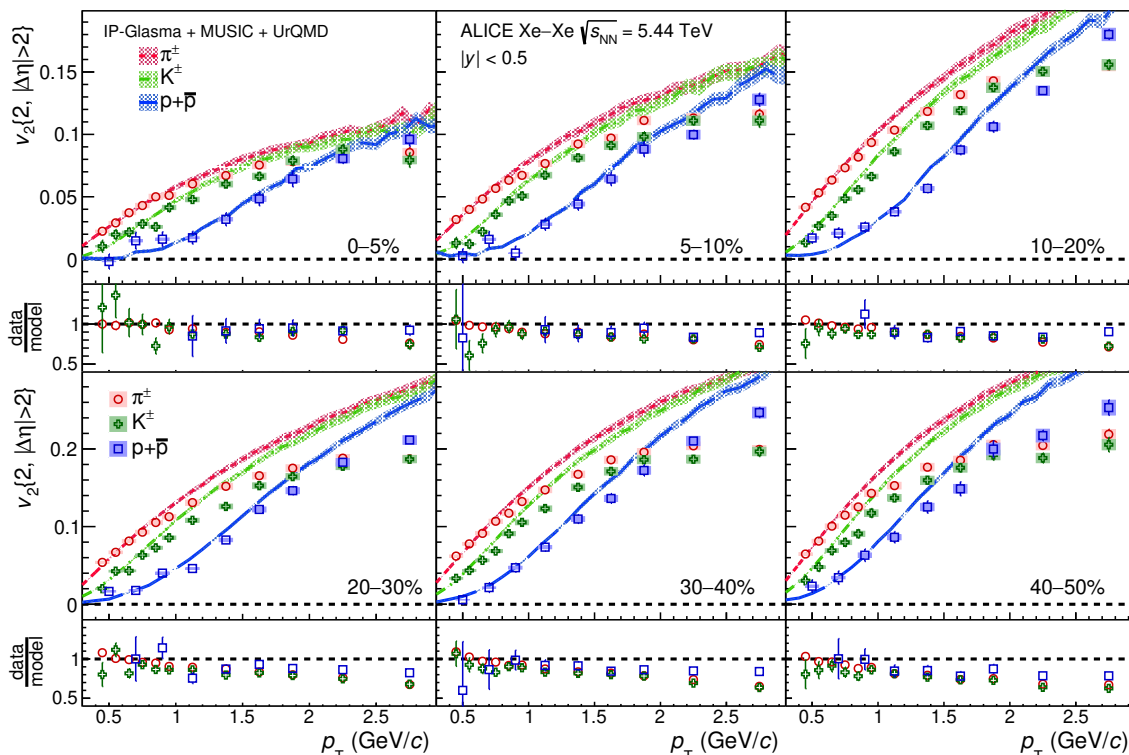
Figure 11. The p_T-differential v_2 of $\pi^\pm$, $K^\pm$, and $p+\overline{p}$ for various centrality classes compared to hydrodynamic calculations from MUSIC model using IP-Glasma initial conditions (colored curves) [67]. Bars (boxes) denote statistical (systematic) uncertainties. The uncertainties of the hydrodynamic calculations are depicted by the thickness of the curves. The ratios of the measured v_2 to a fit to the hydrodynamic calculations are also presented for clarity.

$p+\overline{p}$ is more accurately described than that of $\pi^\pm$ and $K^\pm$ for $p_T \geq 1\,\mathrm{GeV}/c$ in all centrality intervals. A better agreement with the data points is found in central than in peripheral collisions. The differences between the data points and model are also illustrated in figure 11 as the ratios of the measured v_2 to a fit to the theoretical calculations.

4.5 Comparison with v_n of identified particles in Pb-Pb collisions at $\sqrt{s_{NN}} = 5.02\,\mathrm{TeV}$

As mentioned in section 1, the initial state models and transport properties can be further constrained by comparing anisotropic flow coefficients measured in Xe-Xe collisions with those from Pb-Pb collisions. Figures 12 and 13 show the $v_2(p_T)$ and $v_3(p_T)$ of $\pi^\pm$, $K^\pm$, p+$\overline{p}$, K_S^0, and $\Lambda+\overline{\Lambda}$ compared with ALICE measurements performed in Pb-Pb collisions at $\sqrt{s_{NN}} = 5.02\,\mathrm{TeV}$ [32] for various centrality intervals. The v_n coefficients from Pb-Pb collisions were measured employing the same procedure as described in section 2, resulting in similar non-flow contributions to v_n. Ratios of the measurements presented in this paper to a cubic spline fit to the ones performed in Pb-Pb collisions are also given in the figures for each presented centrality interval. The uncertainties in these ratios are obtained by summing the statistical and systematic uncertainties on the Xe-Xe and Pb-Pb measurements in quadrature, and propagating the obtained uncertainties as uncorrelated.
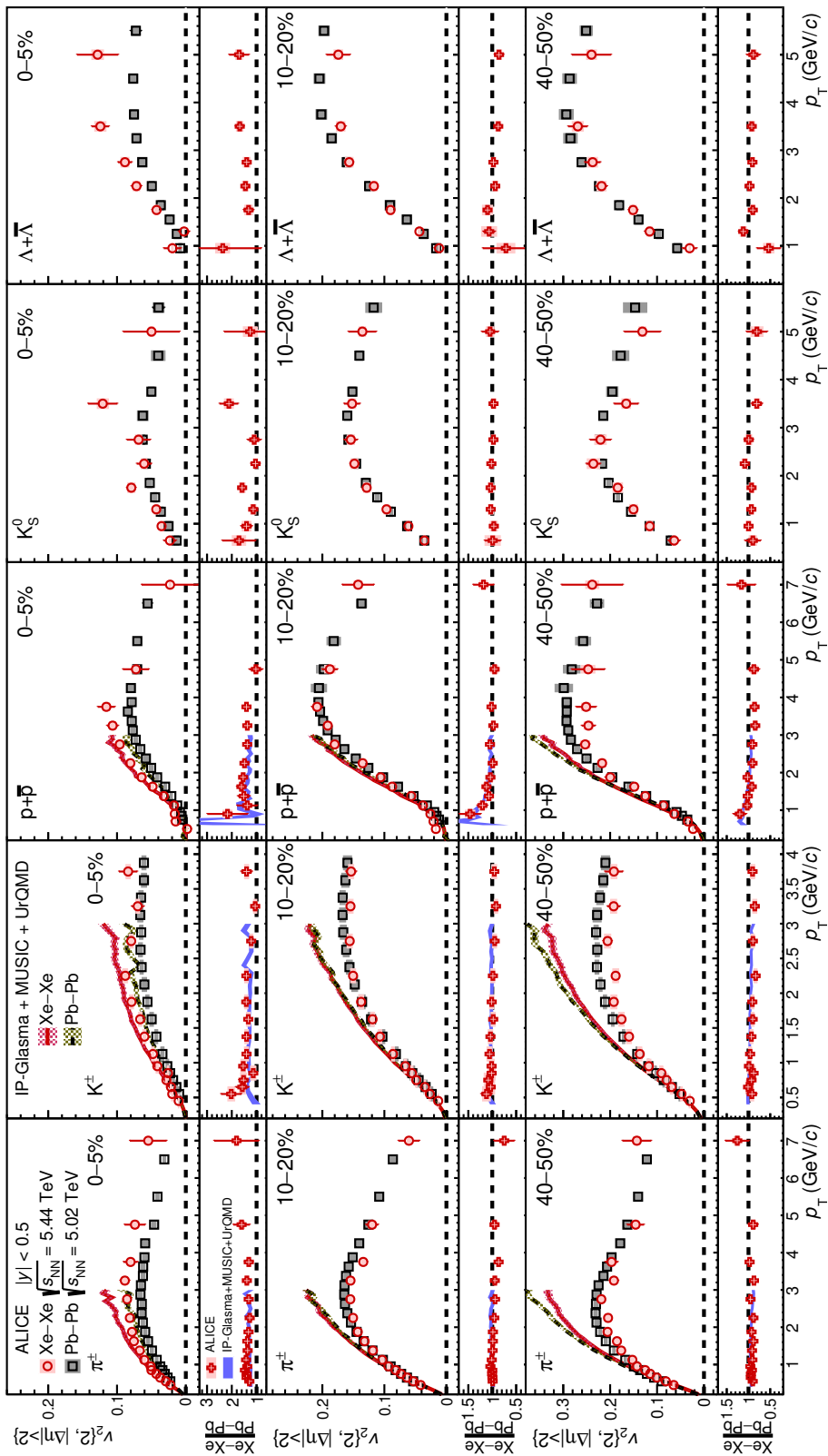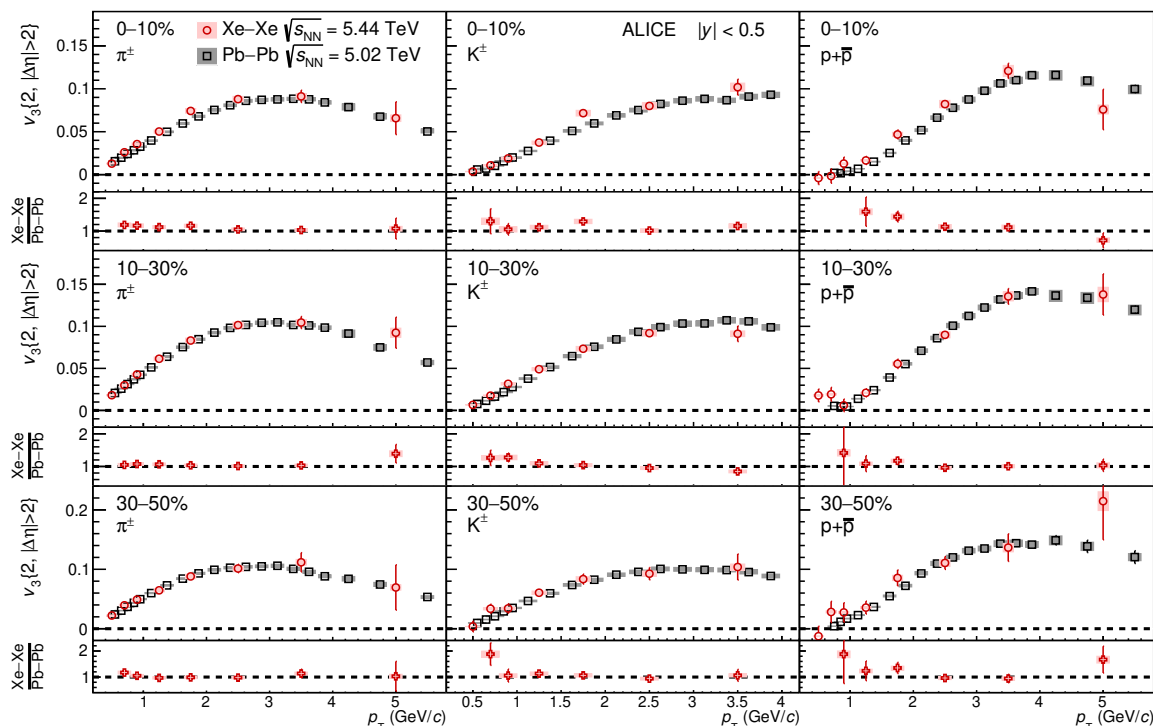
Figure 12. The p_T-differential v_2 of $\pi^\pm$, $K^\pm$, $p+\bar{p}$, K^0_S, and $\Lambda+\bar{\Lambda}$ (red markers) compared to ALICE measurements performed in Pb-Pb collisions at $\sqrt{s_{NN}} = 5.02$ TeV [32] (black markers) for the 0–5% (top panels), 10–20% (middle panels), and 40–50% (bottom panels) centrality intervals. The ratios of Xe-Xe measurements to a cubic spline fit to Pb-Pb measurements are also presented for clarity. The colored curves represent hydrodynamic calculations from MUSIC model using IP-Glasma initial conditions [67]. Bars (boxes) denote statistical (systematic) uncertainties. The uncertainties of the hydrodynamic calculations are depicted by the thickness of the curves.

Figure 13. The p_T-differential v_3 of $\pi^\pm$, $K^\pm$, and p+$\overline{\text{p}}$ (black markers) compared to ALICE measurements performed in Pb-Pb collisions at $\sqrt{s_{NN}} = 5.02$ TeV [32] (red markers) for the 0–10% (top panels), 10–30% (middle panels), and 30–50% (bottom panels) centrality classes. The ratios of Xe-Xe measurements to a cubic spline fit to Pb-Pb measurements are also presented for clarity. Bars (boxes) denote statistical (systematic) uncertainties.

The v_n coefficients at low p_T are expected to be smaller in Pb-Pb collisions than the corresponding Xe-Xe results due to a larger radial flow in the former, an effect which would be most pronounced in central collisions and for heavier particles. However, the v_2 of all particle species in Xe-Xe collisions is systematically above that from Pb-Pb in the entire p_T range in the 0–5% centrality class. The ratios do not depend significantly on p_T and particle species within uncertainties, showing ∼37% larger Xe-Xe values. In terms of the initial state, two effects can be responsible for this behaviour. The first relates to the fact that the ^{208}Pb nucleus is spherical while the ^{129}Xe nucleus is deformed with parameters of the nuclear-charge density distribution not yet measured directly but extrapolated from neighboring isotopes or predicted (the deformation parameter β_2 is predicted to be 0.162 in ref. [75] and extrapolated to 0.18 ± 0.02 in ref. [54]). The second involves initial-state fluctuations being proportional to $A^{-1/2}$ [76], where A is the mass number, and the dependence of $\varepsilon_n\{2\}$ on the number of sources contributing to it which decreases when the number of sources increases [76, 77]. These effects imply larger values of $\varepsilon_2\{2\}$ for central Xe-Xe collisions than central Pb-Pb collisions, which in turn induce larger v_2. However, viscosity is expected to be larger for Xe-Xe collisions as it is proportional to $A^{-1/3}$ [78] which will decrease v_2 [79]. For the 10–20% centrality interval, the measurements are compatible within uncertainties for the different particle species although a possible suppression of
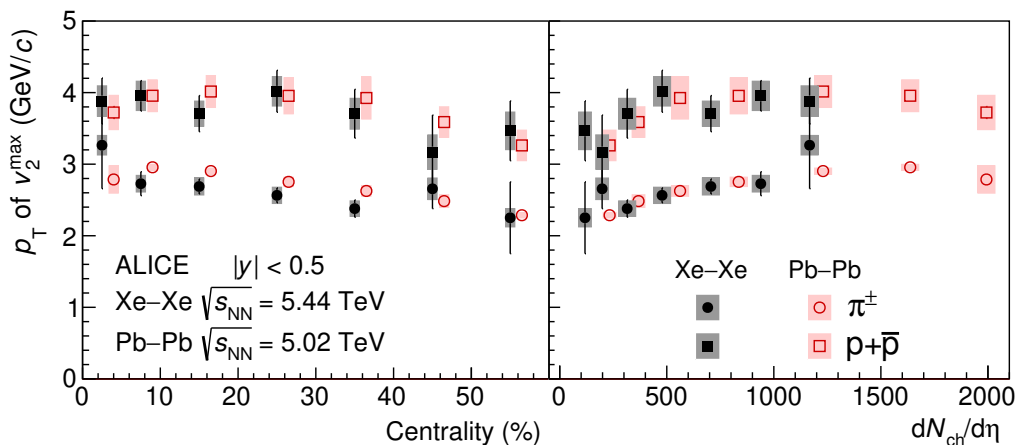
Figure 14. The $p_T|_{v_2^{max}}$ for $\pi^\pm$ and p+$\overline{p}$ (black markers) compared to ALICE measurements performed in Pb-Pb collisions at $\sqrt{s_{NN}} = 5.02\,\mathrm{TeV}$ [32] (red markers) as a function of centrality (left) and charged-particle density (right) [73, 74]. The Pb-Pb points are slightly shifted along the horizontal axis for better visibility in both panels. Bars (boxes) denote statistical (systematic) uncertainties.

p+$\overline{p}$ v_2 from Pb-Pb collisions can be seen for $p_T < 1.5$ GeV/c. For the 40–50% centrality class, no differences are observed between the K_S^0 and $\Lambda+\overline{\Lambda}$ $v_2(p_T)$ measured in the two systems within uncertainties, while the v_2 of $\pi^\pm$, $K^\pm$, and p+$\overline{p}$ from Xe-Xe collisions is ∼8% lower than the corresponding Pb-Pb results. This difference is almost independent of p_T within uncertainties although a possible gradual decrease with increasing p_T up to 2 GeV/c can be seen for p+$\overline{p}$. The larger v_2 values in Pb-Pb collisions might be explained by viscous effects related to the different radial flow and transverse size of the systems since the $\varepsilon_2\{2\}$ coefficients are similar in this centrality interval (differences within 1%) [25, 26]. Although v_3 is expected to be larger in Xe-Xe compared to Pb-Pb due to larger values of $\varepsilon_3\{2\}$ in the same centrality interval [25, 26], the precision of the results does not allow for conclusions to be drawn. The ratios are close to 1 with no significant p_T dependence within uncertainties, except for $\pi^\pm$ and p+$\overline{p}$ v_3 for $p_T < 2$ GeV/c in the 0–10% centrality class.

The $v_2(p_T)$ of $\pi^\pm$, $K^\pm$, and p+$\overline{p}$ measured in Xe-Xe and Pb-Pb collisions is also compared with MUSIC hydrodynamic calculations [67] in figure 12. It is worth noting that these calculations employ the same parameters for Xe-Xe and Pb-Pb collisions (see section 4.4). The Pb-Pb calculations show similar trends to those reported for Xe-Xe collisions: they are in agreement with the measurements for $p_T < 1$ GeV/c and overestimate the data points at higher p_T. However, the MUSIC Xe-Xe/Pb-Pb v_2 ratios quantitatively reproduce the ones of the measurements up to $p_T = 3$ GeV/c. This points to similar differences between the data points and model for both systems. Two potential sources might be responsible for this behavior: improper δf corrections, which are introduced in hydrodynamic models to account for non equilibrium processes at freeze-out and are highly model dependent [80], or sub-optimal tunes of η/s and ζ/s.

Figure 14 shows the value of $p_T|_{v_2^{max}}$ of $\pi^\pm$ and p+$\overline{p}$ and compares these to the ALICE measurements performed in Pb-Pb collisions at $\sqrt{s_{NN}} = 5.02\,\mathrm{TeV}$ [32] as function of

centrality and charged-particle density [73, 74]. For all centrality intervals, the $p_T|_{v_2^{max}}$ of p+$\overline{p}$ has similar values in the two collision systems, within uncertainties. The $p_T|_{v_2^{max}}$ of $\pi^{\pm}$ is slightly lower in Xe-Xe collisions in the 5–40% centrality range. This can be attributed to a different quark density and radial flow at the same centrality in the two systems. Indeed, the $p_T|_{v_2^{max}}$ is the same in Xe-Xe and Pb-Pb collisions for the different particle species within uncertainties when reported as function of charged-particle density.

5 Summary

The elliptic and triangular flow coefficients of $\pi^{\pm}$, K$^{\pm}$, p+$\overline{p}$, K$_S^0$, and $\Lambda+\overline{\Lambda}$ were measured in Xe-Xe collisions at $\sqrt{s_{NN}} = 5.44\,\text{TeV}$. The magnitude of v_2 increases strongly with decreasing centrality up to the 40–50% centrality interval for all particle species, while v_3 shows a weak centrality dependence with a smaller increase than for v_2. This indicates that collision geometry dominates the generation of elliptic flow while triangular flow is generated by event-by-event fluctuations in the initial nucleon and gluon densities. For $p_T < 3\,\text{GeV}/c$, the v_n coefficients show a mass ordering which can be attributed to the interplay between anisotropic flow and radial flow. In this transverse momentum range, MUSIC hydrodynamic calculations reproduce the measured v_2 of $\pi^{\pm}$, K$^{\pm}$, and p+$\overline{p}$ for $p_T < 1\,\text{GeV}/c$. At intermediate transverse momenta ($3 < p_T < 8\,\text{GeV}/c$), the baryon v_n has a magnitude larger than that of mesons, indicating that the particle type dependence persists up to high p_T. Furthermore, particles show an approximate grouping by the number of constituent quarks at the level of $\pm 20\%$ for v_2. The centrality dependence of the shape evolution of $v_2(p_T)$ is different for $\pi^{\pm}$, K$^{\pm}$, and p+$\overline{p}$ for $p_T < 2\,\text{GeV}/c$, being more pronounced for p+$\overline{p}$, but shows no particle type dependence within uncertainties for $p_T \geq 2\,\text{GeV}/c$. Comparing these measurements to those from Pb-Pb collisions at $\sqrt{s_{NN}} = 5.02\,\text{TeV}$, v_2 is larger in central collisions at the same centrality and it has smaller value in peripheral collisions.

References

[1] S.A. Bass, M. Gyulassy, H. Stoecker and W. Greiner, *Signatures of quark gluon plasma formation in high-energy heavy ion collisions: A Critical review*, *J. Phys. G* **25** (1999) R1 [hep-ph/9810281] [INSPIRE].

[2] J.-Y. Ollitrault, *Anisotropy as a signature of transverse collective flow*, *Phys. Rev. D* **46** (1992) 229 [INSPIRE].

[3] S. Voloshin and Y. Zhang, *Flow study in relativistic nuclear collisions by Fourier expansion of Azimuthal particle distributions*, *Z. Phys. C* **70** (1996) 665 [hep-ph/9407282] [INSPIRE].

[4] A.M. Poskanzer and S.A. Voloshin, *Methods for analyzing anisotropic flow in relativistic nuclear collisions*, *Phys. Rev. C* **58** (1998) 1671 [nucl-ex/9805001] [INSPIRE].

[5] R.S. Bhalerao and J.-Y. Ollitrault, *Eccentricity fluctuations and elliptic flow at RHIC*, *Phys. Lett. B* **641** (2006) 260 [nucl-th/0607009] [INSPIRE].

[6] PHOBOS collaboration, *Importance of correlations and fluctuations on the initial source eccentricity in high-energy nucleus-nucleus collisions*, *Phys. Rev. C* **77** (2008) 014906 [arXiv:0711.3724] [INSPIRE].

[7] J. Takahashi et al., *Topology studies of hydrodynamics using two particle correlation analysis*, *Phys. Rev. Lett.* **103** (2009) 242301 [arXiv:0902.4870] [INSPIRE].

[8] B. Alver and G. Roland, *Collision geometry fluctuations and triangular flow in heavy-ion collisions*, *Phys. Rev. C* **81** (2010) 054905 [*Erratum ibid.* **82** (2010) 039903] [arXiv:1003.0194] [INSPIRE].

[9] B.H. Alver, C. Gombeaud, M. Luzum and J.-Y. Ollitrault, *Triangular flow in hydrodynamics and transport theory*, *Phys. Rev. C* **82** (2010) 034913 [arXiv:1007.5469] [INSPIRE].

[10] F.G. Gardim, F. Grassi, M. Luzum and J.-Y. Ollitrault, *Mapping the hydrodynamic response to the initial geometry in heavy-ion collisions*, *Phys. Rev. C* **85** (2012) 024908 [arXiv:1111.6538] [INSPIRE].

[11] G.-Y. Qin, H. Petersen, S.A. Bass and B. Müller, *Translation of collision geometry fluctuations into momentum anisotropies in relativistic heavy-ion collisions*, *Phys. Rev. C* **82** (2010) 064903 [arXiv:1009.1847] [INSPIRE].

[12] D. Teaney and L. Yan, *Triangularity and Dipole Asymmetry in Heavy Ion Collisions*, *Phys. Rev. C* **83** (2011) 064904 [arXiv:1010.1876] [INSPIRE].

[13] BRAHMS collaboration, *Quark gluon plasma and color glass condensate at RHIC? The Perspective from the BRAHMS experiment*, *Nucl. Phys. A* **757** (2005) 1 [nucl-ex/0410020] [INSPIRE].

[14] PHENIX collaboration, *Formation of dense partonic matter in relativistic nucleus-nucleus collisions at RHIC: Experimental evaluation by the PHENIX collaboration*, *Nucl. Phys. A* **757** (2005) 184 [nucl-ex/0410003] [INSPIRE].

[15] PHOBOS collaboration, *The PHOBOS perspective on discoveries at RHIC*, *Nucl. Phys. A* **757** (2005) 28 [nucl-ex/0410022] [INSPIRE].

[16] STAR collaboration, *Experimental and theoretical challenges in the search for the quark gluon plasma: The STAR Collaboration's critical assessment of the evidence from RHIC collisions*, *Nucl. Phys. A* **757** (2005) 102 [`nucl-ex/0501009`] [ɪɴSPIRE].

[17] ALICE collaboration, *Higher harmonic anisotropic flow measurements of charged particles in Pb-Pb collisions at $\sqrt{s_{\mathrm{NN}}} = 2.76$ TeV*, *Phys. Rev. Lett.* **107** (2011) 032301 [`arXiv:1105.3865`] [ɪɴSPIRE].

[18] ALICE collaboration, *Energy dependence and fluctuations of anisotropic flow in Pb-Pb collisions at $\sqrt{s_{\mathrm{NN}}} = 5.02$ and 2.76 TeV*, *JHEP* **07** (2018) 103 [`arXiv:1804.02944`] [ɪɴSPIRE].

[19] ATLAS collaboration, *Measurement of the azimuthal anisotropy for charged particle production in $\sqrt{s_{\mathrm{NN}}} = 2.76$ TeV lead-lead collisions with the ATLAS detector*, *Phys. Rev. C* **86** (2012) 014907 [`arXiv:1203.3087`] [ɪɴSPIRE].

[20] CMS collaboration, *Measurement of Higher-Order Harmonic Azimuthal Anisotropy in PbPb Collisions at $\sqrt{s_{\mathrm{NN}}} = 2.76$ TeV*, *Phys. Rev. C* **89** (2014) 044906 [`arXiv:1310.8651`] [ɪɴSPIRE].

[21] P. Kovtun, D.T. Son and A.O. Starinets, *Viscosity in strongly interacting quantum field theories from black hole physics*, *Phys. Rev. Lett.* **94** (2005) 111601 [`hep-th/0405231`] [ɪɴSPIRE].

[22] ALICE collaboration, *Anisotropic flow in Xe-Xe collisions at $\sqrt{s_{\mathrm{NN}}} = 5.44$ TeV*, *Phys. Lett. B* **784** (2018) 82 [`arXiv:1805.01832`] [ɪɴSPIRE].

[23] CMS collaboration, *Charged-particle angular correlations in XeXe collisions at $\sqrt{s_{\mathrm{NN}}} = 5.44$ TeV*, *Phys. Rev. C* **100** (2019) 044902 [`arXiv:1901.07997`] [ɪɴSPIRE].

[24] ATLAS collaboration, *Measurement of the azimuthal anisotropy of charged-particle production in $Xe+Xe$ collisions at $\sqrt{s_{\mathrm{NN}}} = 5.44$ TeV with the ATLAS detector*, *Phys. Rev. C* **101** (2020) 024906 [`arXiv:1911.04812`] [ɪɴSPIRE].

[25] G. Giacalone, J. Noronha-Hostler, M. Luzum and J.-Y. Ollitrault, *Hydrodynamic predictions for 5.44 TeV Xe+Xe collisions*, *Phys. Rev. C* **97** (2018) 034904 [`arXiv:1711.08499`] [ɪɴSPIRE].

[26] K.J. Eskola, H. Niemi, R. Paatelainen and K. Tuominen, *Predictions for multiplicities and flow harmonics in 5.44 TeV Xe+Xe collisions at the CERN Large Hadron Collider*, *Phys. Rev. C* **97** (2018) 034911 [`arXiv:1711.09803`] [ɪɴSPIRE].

[27] Z. Qiu and U.W. Heinz, *Event-by-event shape and flow fluctuations of relativistic heavy-ion collision fireballs*, *Phys. Rev. C* **84** (2011) 024911 [`arXiv:1104.0650`] [ɪɴSPIRE].

[28] P. Huovinen, P.F. Kolb, U.W. Heinz, P.V. Ruuskanen and S.A. Voloshin, *Radial and elliptic flow at RHIC: Further predictions*, *Phys. Lett. B* **503** (2001) 58 [`hep-ph/0101136`] [ɪɴSPIRE].

[29] C. Shen, U. Heinz, P. Huovinen and H. Song, *Radial and elliptic flow in Pb+Pb collisions at the Large Hadron Collider from viscous hydrodynamic*, *Phys. Rev. C* **84** (2011) 044903 [`arXiv:1105.3226`] [ɪɴSPIRE].

[30] ALICE collaboration, *Elliptic flow of identified hadrons in Pb-Pb collisions at $\sqrt{s_{\mathrm{NN}}} = 2.76$ TeV*, *JHEP* **06** (2015) 190 [`arXiv:1405.4632`] [ɪɴSPIRE].

[31] ALICE collaboration, *Higher harmonic flow coefficients of identified hadrons in Pb-Pb collisions at $\sqrt{s_{\mathrm{NN}}} = 2.76$ TeV*, *JHEP* **09** (2016) 164 [`arXiv:1606.06057`] [ɪɴSPIRE].

[32] ALICE collaboration, *Anisotropic flow of identified particles in Pb-Pb collisions at $\sqrt{s_{\mathrm{NN}}} = 5.02$ TeV*, *JHEP* **09** (2018) 006 [`arXiv:1805.04390`] [ɪɴSPIRE].

[33] STAR collaboration, *Particle type dependence of azimuthal anisotropy and nuclear modification of particle production in Au+Au collisions at $\sqrt{s_{NN}} = 200$ GeV*, *Phys. Rev. Lett.* **92** (2004) 052302 [nucl-ex/0306007] [INSPIRE].

[34] PHENIX collaboration, *Elliptic flow of identified hadrons in Au+Au collisions at $\sqrt{s_{NN}} = 200$ GeV*, *Phys. Rev. Lett.* **91** (2003) 182301 [nucl-ex/0305013] [INSPIRE].

[35] ALICE collaboration, *Anisotropic flow of charged hadrons, pions and (anti-)protons measured at high transverse momentum in Pb-Pb collisions at $\sqrt{s_{NN}} = 2.76$ TeV*, *Phys. Lett. B* **719** (2013) 18 [arXiv:1205.5761] [INSPIRE].

[36] STAR collaboration, *Mass, quark-number, and $\sqrt{s_{NN}}$ dependence of the second and fourth flow harmonics in ultra-relativistic nucleus-nucleus collisions*, *Phys. Rev. C* **75** (2007) 054906 [nucl-ex/0701010] [INSPIRE].

[37] PHENIX collaboration, *Deviation from quark-number scaling of the anisotropy parameter v_2 of pions, kaons, and protons in Au+Au collisions at $\sqrt{s_{NN}} = 200$ GeV*, *Phys. Rev. C* **85** (2012) 064914 [arXiv:1203.2644] [INSPIRE].

[38] D. Molnar and S.A. Voloshin, *Elliptic flow at large transverse momenta from quark coalescence*, *Phys. Rev. Lett.* **91** (2003) 092301 [nucl-th/0302014] [INSPIRE].

[39] V. Greco, C.M. Ko and P. Levai, *Parton coalescence at RHIC*, *Phys. Rev. C* **68** (2003) 034904 [nucl-th/0305024] [INSPIRE].

[40] R.J. Fries, B. Müller, C. Nonaka and S.A. Bass, *Hadron production in heavy ion collisions: Fragmentation and recombination from a dense parton phase*, *Phys. Rev. C* **68** (2003) 044902 [nucl-th/0306027] [INSPIRE].

[41] K. Werner, I. Karpenko, M. Bleicher, T. Pierog and S. Porteboeuf-Houssais, *Jets, Bulk Matter, and their Interaction in Heavy Ion Collisions at Several TeV*, *Phys. Rev. C* **85** (2012) 064907 [arXiv:1203.5704] [INSPIRE].

[42] H. Sato and K. Yazaki, *On the coalescence model for high-energy nuclear reactions*, *Phys. Lett. B* **98** (1981) 153 [INSPIRE].

[43] C.B. Dover, U.W. Heinz, E. Schnedermann and J. Zimanyi, *Relativistic coalescence model for high-energy nuclear collisions*, *Phys. Rev. C* **44** (1991) 1636 [INSPIRE].

[44] STAR collaboration, *Elliptic flow from two and four particle correlations in Au+Au collisions at $\sqrt{s_{NN}} = 130$ GeV*, *Phys. Rev. C* **66** (2002) 034904 [nucl-ex/0206001] [INSPIRE].

[45] S.A. Voloshin, A.M. Poskanzer and R. Snellings, *Collective phenomena in non-central nuclear collisions*, *Landolt-Bornstein* **23** (2010) 293 [arXiv:0809.2949] [INSPIRE].

[46] M. Luzum and J.-Y. Ollitrault, *Eliminating experimental bias in anisotropic-flow measurements of high-energy nuclear collisions*, *Phys. Rev. C* **87** (2013) 044907 [arXiv:1209.2323] [INSPIRE].

[47] ALICE collaboration, *The ALICE experiment at the CERN LHC*, 2008 *JINST* **3** S08002 [INSPIRE].

[48] ALICE collaboration, *Performance of the ALICE Experiment at the CERN LHC*, *Int. J. Mod. Phys. A* **29** (2014) 1430044 [arXiv:1402.4476] [INSPIRE].

[49] ALICE collaboration, *Alignment of the ALICE Inner Tracking System with cosmic-ray tracks*, 2010 *JINST* **5** P03003 [arXiv:1001.0502] [INSPIRE].

[50] J. Alme et al., *The ALICE TPC, a large 3-dimensional tracking device with fast readout for ultra-high multiplicity events*, *Nucl. Instrum. Meth. A* **622** (2010) 316 [arXiv:1001.1950] [INSPIRE].

[51] A. Akindinov et al., *Performance of the ALICE Time-Of-Flight detector at the LHC*, *Eur. Phys. J. Plus* **128** (2013) 44 [INSPIRE].

[52] ALICE collaboration, *Performance of the ALICE VZERO system*, 2013 *JINST* **8** P10016 [arXiv:1306.3130] [INSPIRE].

[53] M. Bondila et al., *ALICE T0 detector*, *IEEE Trans. Nucl. Sci.* **52** (2005) 1705 [INSPIRE].

[54] ALICE collaboration, *Centrality determination using the Glauber model in Xe-Xe collisions at* $\sqrt{s_{NN}} = 5.44$ *TeV*, ALICE-PUBLIC-2018-003 (2018).

[55] R. Arnaldi et al., *The Zero degree calorimeters for the ALICE experiment*, *Nucl. Instrum. Meth. A* **581** (2007) 397 [*Erratum ibid.* **604** (2009) 765] [INSPIRE].

[56] ALICE collaboration, *Transverse momentum spectra and nuclear modification factors of charged particles in Xe-Xe collisions at* $\sqrt{s_{NN}} = 5.44$ *TeV*, *Phys. Lett. B* **788** (2019) 166 [arXiv:1805.04399] [INSPIRE].

[57] ALICE collaboration, *Centrality dependence of* π, *K, p production in Pb-Pb collisions at* $\sqrt{s_{NN}} = 2.76$ *TeV*, *Phys. Rev. C* **88** (2013) 044910 [arXiv:1303.0737] [INSPIRE].

[58] J. Podolanski and R. Armenteros, *Iii. analysis of v-events*, *Philos. Mag.* **45** (1954) 13.

[59] I. Selyuzhenkov and S. Voloshin, *Effects of non-uniform acceptance in anisotropic flow measurement*, *Phys. Rev. C* **77** (2008) 034904 [arXiv:0707.4672] [INSPIRE].

[60] N. Borghini and J.Y. Ollitrault, *Azimuthally sensitive correlations in nucleus-nucleus collisions*, *Phys. Rev. C* **70** (2004) 064905 [nucl-th/0407041] [INSPIRE].

[61] R. Barlow, *Systematic errors: Facts and fictions*, in *Conference on Advanced Statistical Techniques in Particle Physics*, pp. 134–144 (2002) [hep-ex/0207026] [INSPIRE].

[62] H. Song and U.W. Heinz, *Suppression of elliptic flow in a minimally viscous quark-gluon plasma*, *Phys. Lett. B* **658** (2008) 279 [arXiv:0709.0742] [INSPIRE].

[63] H. Song, S. Bass and U.W. Heinz, *Spectra and elliptic flow for identified hadrons in 2.76A TeV Pb+Pb collisions*, *Phys. Rev. C* **89** (2014) 034919 [arXiv:1311.0157] [INSPIRE].

[64] ALICE collaboration, *Production of pions, kaons, (anti-)protons and* ϕ *mesons in Xe-Xe collisions at* $\sqrt{s_{NN}} = 5.44$ *TeV*, *Eur. Phys. J. C* **81** (2021) 584 [arXiv:2101.03100] [INSPIRE].

[65] R.J. Fries, V. Greco and P. Sorensen, *Coalescence Models For Hadron Formation From Quark Gluon Plasma*, *Ann. Rev. Nucl. Part. Sci.* **58** (2008) 177 [arXiv:0807.4939] [INSPIRE].

[66] N. Borghini and J.-Y. Ollitrault, *Momentum spectra, anisotropic flow, and ideal fluids*, *Phys. Lett. B* **642** (2006) 227 [nucl-th/0506045] [INSPIRE].

[67] B. Schenke, C. Shen and P. Tribedy, *Running the gamut of high energy nuclear collisions*, *Phys. Rev. C* **102** (2020) 044905 [arXiv:2005.14682] [INSPIRE].

[68] B. Schenke, S. Jeon and C. Gale, *Elliptic and triangular flow in event-by-event* $(3+1)D$ *viscous hydrodynamics*, *Phys. Rev. Lett.* **106** (2011) 042301 [arXiv:1009.3244] [INSPIRE].

[69] B. Schenke, P. Tribedy and R. Venugopalan, *Fluctuating Glasma initial conditions and flow in heavy ion collisions*, *Phys. Rev. Lett.* **108** (2012) 252301 [arXiv:1202.6646] [INSPIRE].

[70] B. Schenke, P. Tribedy and R. Venugopalan, *Event-by-event gluon multiplicity, energy density, and eccentricities in ultrarelativistic heavy-ion collisions*, *Phys. Rev. C* **86** (2012) 034908 [arXiv:1206.6805] [INSPIRE].

[71] S.A. Bass et al., *Microscopic models for ultrarelativistic heavy ion collisions*, *Prog. Part. Nucl. Phys.* **41** (1998) 255 [nucl-th/9803035] [INSPIRE].

[72] M. Bleicher et al., *Relativistic hadron hadron collisions in the ultrarelativistic quantum molecular dynamics model*, *J. Phys. G* **25** (1999) 1859 [hep-ph/9909407] [INSPIRE].

[73] ALICE collaboration, *Centrality dependence of the charged-particle multiplicity density at midrapidity in Pb-Pb collisions at $\sqrt{s_{\rm NN}} = 5.02$ TeV*, *Phys. Rev. Lett.* **116** (2016) 222302 [arXiv:1512.06104] [INSPIRE].

[74] ALICE collaboration, *Centrality and pseudorapidity dependence of the charged-particle multiplicity density in Xe-Xe collisions at $\sqrt{s_{\rm NN}} = 5.44$ TeV*, *Phys. Lett. B* **790** (2019) 35 [arXiv:1805.04432] [INSPIRE].

[75] P. Möller, A.J. Sierk, T. Ichikawa and H. Sagawa, *Nuclear ground-state masses and deformations: FRDM(2012)*, *Atom. Data Nucl. Data Tabl.* **109-110** (2016) 1 [arXiv:1508.06294] [INSPIRE].

[76] R.S. Bhalerao, M. Luzum and J.-Y. Ollitrault, *Understanding anisotropy generated by fluctuations in heavy-ion collisions*, *Phys. Rev. C* **84** (2011) 054901 [arXiv:1107.5485] [INSPIRE].

[77] A. Bzdak, P. Bozek and L. McLerran, *Fluctuation induced equality of multi-particle eccentricities for four or more particles*, *Nucl. Phys. A* **927** (2014) 15 [arXiv:1311.7325] [INSPIRE].

[78] R. Baier, P. Romatschke, D.T. Son, A.O. Starinets and M.A. Stephanov, *Relativistic viscous hydrodynamics, conformal invariance, and holography*, *JHEP* **04** (2008) 100 [arXiv:0712.2451] [INSPIRE].

[79] P. Romatschke and U. Romatschke, *Viscosity Information from Relativistic Nuclear Collisions: How Perfect is the Fluid Observed at RHIC?*, *Phys. Rev. Lett.* **99** (2007) 172301 [arXiv:0706.1522] [INSPIRE].

[80] J. Noronha-Hostler, J. Noronha and F. Grassi, *Bulk viscosity-driven suppression of shear viscosity effects on the flow harmonics at energies available at the BNL Relativistic Heavy Ion Collider*, *Phys. Rev. C* **90** (2014) 034907 [arXiv:1406.3333] [INSPIRE].

...
The ALICE collaboration

S. Acharya[141], D. Adamová[96], A. Adler[74], G. Aglieri Rinella[34], M. Agnello[30], N. Agrawal[54],
Z. Ahammed[141], S. Ahmad[16], S.U. Ahn[76], I. Ahuja[38], Z. Akbar[51], A. Akindinov[93],
M. Al-Turany[108], S.N. Alam[16,40], D. Aleksandrov[89], B. Alessandro[59], H.M. Alfanda[7],
R. Alfaro Molina[71], B. Ali[16], Y. Ali[14], A. Alici[25], N. Alizadehvandchali[125], A. Alkin[34],
J. Alme[21], T. Alt[68], L. Altenkamper[21], I. Altsybeev[113], M.N. Anaam[7], C. Andrei[48],
D. Andreou[91], A. Andronic[144], M. Angeletti[34], V. Anguelov[105], F. Antinori[57],
P. Antonioli[54], C. Anuj[16], N. Apadula[80], L. Aphecetche[115], H. Appelshäuser[68], S. Arcelli[25],
R. Arnaldi[59], I.C. Arsene[20], M. Arslandok[146,105], A. Augustinus[34], R. Averbeck[108],
S. Aziz[78], M.D. Azmi[16], A. Badalà[56], Y.W. Baek[41], X. Bai[129,108], R. Bailhache[68],
Y. Bailung[50], R. Bala[102], A. Balbino[30], A. Baldisseri[138], B. Balis[2], M. Ball[43], D. Banerjee[4],
R. Barbera[26], L. Barioglio[106], M. Barlou[85], G.G. Barnaföldi[145], L.S. Barnby[95],
V. Barret[135], C. Bartels[128], K. Barth[34], E. Bartsch[68], F. Baruffaldi[27], N. Bastid[135],
S. Basu[81], G. Batigne[115], B. Batyunya[75], D. Bauri[49], J.L. Bazo Alba[112], I.G. Bearden[90],
C. Beattie[146], I. Belikov[137], A.D.C. Bell Hechavarria[144], F. Bellini[25], R. Bellwied[125],
S. Belokurova[113], V. Belyaev[94], G. Bencedi[69], S. Beole[24], A. Bercuci[48], Y. Berdnikov[99],
A. Berdnikova[105], L. Bergmann[105], M.G. Besoiu[67], L. Betev[34], P.P. Bhaduri[141],
A. Bhasin[102], I.R. Bhat[102], M.A. Bhat[4], B. Bhattacharjee[42], P. Bhattacharya[22],
L. Bianchi[24], N. Bianchi[52], J. Bielčík[37], J. Bielčíková[96], J. Biernat[118], A. Bilandzic[106],
G. Biro[145], S. Biswas[4], J.T. Blair[119], D. Blau[89,82], M.B. Blidaru[108], C. Blume[68],
G. Boca[28,58], F. Bock[97], A. Bogdanov[94], S. Boi[22], J. Bok[61], L. Boldizsár[145],
A. Bolozdynya[94], M. Bombara[38], P.M. Bond[34], G. Bonomi[140,58], H. Borel[138], A. Borissov[82],
H. Bossi[146], E. Botta[24], L. Bratrud[68], P. Braun-Munzinger[108], M. Bregant[121], M. Broz[37],
G.E. Bruno[107,33], M.D. Buckland[128], D. Budnikov[109], H. Buesching[68], S. Bufalino[30],
O. Bugnon[115], P. Buhler[114], Z. Buthelezi[72,132], J.B. Butt[14], S.A. Bysiak[118], M. Cai[27,7],
H. Caines[146], A. Caliva[108], E. Calvo Villar[112], J.M.M. Camacho[120], R.S. Camacho[45],
P. Camerini[23], F.D.M. Canedo[121], F. Carnesecchi[34,25], R. Caron[138],
J. Castillo Castellanos[138], E.A.R. Casula[22], F. Catalano[30], C. Ceballos Sanchez[75],
P. Chakraborty[49], S. Chandra[141], S. Chapeland[34], M. Chartier[128], S. Chattopadhyay[141],
S. Chattopadhyay[110], A. Chauvin[22], T.G. Chavez[45], T. Cheng[7], C. Cheshkov[136],
B. Cheynis[136], V. Chibante Barroso[34], D.D. Chinellato[122], S. Cho[61], P. Chochula[34],
P. Christakoglou[91], C.H. Christensen[90], P. Christiansen[81], T. Chujo[134], C. Cicalo[55],
L. Cifarelli[25], F. Cindolo[54], M.R. Ciupek[108], G. Clai[II,54], J. Cleymans[I,124], F. Colamaria[53],
J.S. Colburn[111], D. Colella[107,53,33,145], A. Collu[80], M. Colocci[34], M. Concas[III,59],
G. Conesa Balbastre[79], Z. Conesa del Valle[78], G. Contin[23], J.G. Contreras[37],
M.L. Coquet[138], T.M. Cormier[97], P. Cortese[31], M.R. Cosentino[123], F. Costa[34],
S. Costanza[28,58], P. Crochet[135], R. Cruz-Torres[80], E. Cuautle[69], P. Cui[7], L. Cunqueiro[97],
A. Dainese[57], M.C. Danisch[105], A. Danu[67], I. Das[110], P. Das[87], P. Das[4], S. Das[4], S. Dash[49],
S. De[87], A. De Caro[29], G. de Cataldo[53], L. De Cilladi[24], J. de Cuveland[39], A. De Falco[22],
D. De Gruttola[29], N. De Marco[59], C. De Martin[23], S. De Pasquale[29], S. Deb[50],
H.F. Degenhardt[121], K.R. Deja[142], L. Dello Stritto[29], S. Delsanto[24], W. Deng[7],
P. Dhankher[19], D. Di Bari[33], A. Di Mauro[34], R.A. Diaz[8], T. Dietel[124], Y. Ding[136,7],

R. Divià[34], D.U. Dixit[19], Ø. Djuvsland[21], U. Dmitrieva[63], J. Do[61], A. Dobrin[67],
B. Dönigus[68], O. Dordic[20], A.K. Dubey[141], A. Dubla[108,91], S. Dudi[101], M. Dukhishyam[87],
P. Dupieux[135], N. Dzalaiova[13], T.M. Eder[144], R.J. Ehlers[97], V.N. Eikeland[21],
F. Eisenhut[68], D. Elia[53], B. Erazmus[115], F. Ercolessi[25], F. Erhardt[100], A. Erokhin[113],
M.R. Ersdal[21], B. Espagnon[78], G. Eulisse[34], D. Evans[111], S. Evdokimov[92], L. Fabbietti[106],
M. Faggin[27], J. Faivre[79], F. Fan[7], A. Fantoni[52], M. Fasel[97], P. Fecchio[30], A. Feliciello[59],
G. Feofilov[113], A. Fernández Téllez[45], A. Ferrero[138], A. Ferretti[24], V.J.G. Feuillard[105],
J. Figiel[118], S. Filchagin[109], D. Finogeev[63], F.M. Fionda[55,21], G. Fiorenza[34,107], F. Flor[125],
A.N. Flores[119], S. Foertsch[72], P. Foka[108], S. Fokin[89], E. Fragiacomo[60], E. Frajna[145],
U. Fuchs[34], N. Funicello[29], C. Furget[79], A. Furs[63], J.J. Gaardhøje[90], M. Gagliardi[24],
A.M. Gago[112], A. Gal[137], C.D. Galvan[120], P. Ganoti[85], C. Garabatos[108], J.R.A. Garcia[45],
E. Garcia-Solis[10], K. Garg[115], C. Gargiulo[34], A. Garibli[88], K. Garner[144], P. Gasik[108],
E.F. Gauger[119], A. Gautam[127], M.B. Gay Ducati[70], M. Germain[115], P. Ghosh[141],
S.K. Ghosh[4], M. Giacalone[25], P. Gianotti[52], P. Giubellino[108,59], P. Giubilato[27],
A.M.C. Glaenzer[138], P. Glässel[105], D.J.Q. Goh[83], V. Gonzalez[143], L.H. González-Trueba[71],
S. Gorbunov[39], M. Gorgon[2], L. Görlich[118], S. Gotovac[35], V. Grabski[71],
L.K. Graczykowski[142], L. Greiner[80], A. Grelli[62], C. Grigoras[34], V. Grigoriev[94],
S. Grigoryan[75,1], O.S. Groettvik[21], F. Grosa[34,59], J.F. Grosse-Oetringhaus[34], R. Grosso[108],
G.G. Guardiano[122], R. Guernane[79], M. Guilbaud[115], K. Gulbrandsen[90], T. Gunji[133],
W. Guo[7], A. Gupta[102], R. Gupta[102], S.P. Guzman[45], L. Gyulai[145], M.K. Habib[108],
C. Hadjidakis[78], G. Halimoglu[68], H. Hamagaki[83], G. Hamar[145], M. Hamid[7],
R. Hannigan[119], M.R. Haque[142,87], A. Harlenderova[108], J.W. Harris[146], A. Harton[10],
J.A. Hasenbichler[34], H. Hassan[97], D. Hatzifotiadou[54], P. Hauer[43], L.B. Havener[146],
S. Hayashi[133], S.T. Heckel[106], E. Hellbär[108], H. Helstrup[36], T. Herman[37],
E.G. Hernandez[45], G. Herrera Corral[9], F. Herrmann[144], K.F. Hetland[36], H. Hillemanns[34],
C. Hills[128], B. Hippolyte[137], B. Hofman[62], B. Hohlweger[91], J. Honermann[144],
G.H. Hong[147], D. Horak[37], S. Hornung[108], A. Horzyk[2], R. Hosokawa[15], Y. Hou[7],
P. Hristov[34], C. Hughes[131], P. Huhn[68], T.J. Humanic[98], H. Hushnud[110], L.A. Husova[144],
A. Hutson[125], D. Hutter[39], J.P. Iddon[34,128], R. Ilkaev[109], H. Ilyas[14], M. Inaba[134],
G.M. Innocenti[34], M. Ippolitov[89], A. Isakov[37,96], M.S. Islam[110], M. Ivanov[108], V. Ivanov[99],
V. Izucheev[92], M. Jablonski[2], B. Jacak[80], N. Jacazio[34], P.M. Jacobs[80], S. Jadlovska[117],
J. Jadlovsky[117], S. Jaelani[62], C. Jahnke[122,121], M.J. Jakubowska[142], A. Jalotra[102],
M.A. Janik[142], T. Janson[74], M. Jercic[100], O. Jevons[111], A.A.P. Jimenez[69], F. Jonas[97,144],
P.G. Jones[111], J.M. Jowett[34,108], J. Jung[68], M. Jung[68], A. Junique[34], A. Jusko[111],
J. Kaewjai[116], P. Kalinak[64], A. Kalweit[34], V. Kaplin[94], S. Kar[7], A. Karasu Uysal[77],
D. Karatovic[100], O. Karavichev[63], T. Karavicheva[63], P. Karczmarczyk[142], E. Karpechev[63],
A. Kazantsev[89], U. Kebschull[74], R. Keidel[47], D.L.D. Keijdener[62], M. Keil[34], B. Ketzer[43],
Z. Khabanova[91], A.M. Khan[7], S. Khan[16], A. Khanzadeev[99], Y. Kharlov[92,82], A. Khatun[16],
A. Khuntia[118], B. Kileng[36], B. Kim[17,61], C. Kim[17], D.J. Kim[126], E.J. Kim[73], J. Kim[147],
J.S. Kim[41], J. Kim[105], J. Kim[147], J. Kim[73], M. Kim[105], S. Kim[18], T. Kim[147], S. Kirsch[68],
I. Kisel[39], S. Kiselev[93], A. Kisiel[142], J.P. Kitowski[2], J.L. Klay[6], J. Klein[34], S. Klein[80],
C. Klein-Bösing[144], M. Kleiner[68], T. Klemenz[106], A. Kluge[34], A.G. Knospe[125],
C. Kobdaj[116], M.K. Köhler[105], T. Kollegger[108], A. Kondratyev[75], N. Kondratyeva[94],

E. Kondratyuk[92], J. Konig[68], S.A. Konigstorfer[106], P.J. Konopka[34,2], G. Kornakov[142],
S.D. Koryciak[2], L. Koska[117], A. Kotliarov[96], O. Kovalenko[86], V. Kovalenko[113],
M. Kowalski[118], I. Králik[64], A. Kravčáková[38], L. Kreis[108], M. Krivda[111,64], F. Krizek[96],
K. Krizkova Gajdosova[37], M. Kroesen[105], M. Krüger[68], E. Kryshen[99], M. Krzewicki[39],
V. Kučera[34], C. Kuhn[137], P.G. Kuijer[91], T. Kumaoka[134], D. Kumar[141], L. Kumar[101],
N. Kumar[101], S. Kundu[34,87], P. Kurashvili[86], A. Kurepin[63], A.B. Kurepin[63],
A. Kuryakin[109], S. Kushpil[96], J. Kvapil[111], M.J. Kweon[61], J.Y. Kwon[61], Y. Kwon[147],
S.L. La Pointe[39], P. La Rocca[26], Y.S. Lai[80], A. Lakrathok[116], M. Lamanna[34],
R. Langoy[130], K. Lapidus[34], P. Larionov[34,52], E. Laudi[34], L. Lautner[34,106], R. Lavicka[37],
T. Lazareva[113], R. Lea[140,23,58], J. Lehrbach[39], R.C. Lemmon[95], I. León Monzón[120],
E.D. Lesser[19], M. Lettrich[34,106], P. Lévai[145], X. Li[11], X.L. Li[7], J. Lien[130], R. Lietava[111],
B. Lim[17], S.H. Lim[17], V. Lindenstruth[39], A. Lindner[48], C. Lippmann[108], A. Liu[19],
D.H. Liu[7], J. Liu[128], I.M. Lofnes[21], V. Loginov[94], C. Loizides[97], P. Loncar[35], J.A. Lopez[105],
X. Lopez[135], E. López Torres[8], J.R. Luhder[144], M. Lunardon[27], G. Luparello[60], Y.G. Ma[40],
A. Maevskaya[63], M. Mager[34], T. Mahmoud[43], A. Maire[137], M. Malaev[99], N.M. Malik[102],
Q.W. Malik[20], L. Malinina[IV,75], D. Mal'Kevich[93], N. Mallick[50], P. Malzacher[108],
G. Mandaglio[32,56], V. Manko[89], F. Manso[135], V. Manzari[53], Y. Mao[7], J. Mareš[66],
G.V. Margagliotti[23], A. Margotti[54], A. Marín[108], C. Markert[119], M. Marquard[68],
N.A. Martin[105], P. Martinengo[34], J.L. Martinez[125], M.I. Martínez[45], G. Martínez García[115],
S. Masciocchi[108], M. Masera[24], A. Masoni[55], L. Massacrier[78], A. Mastroserio[139,53],
A.M. Mathis[106], O. Matonoha[81], P.F.T. Matuoka[121], A. Matyja[118], C. Mayer[118],
A.L. Mazuecos[34], F. Mazzaschi[24], M. Mazzilli[34], J.E. Mdhluli[132], A.F. Mechler[68],
Y. Melikyan[63], A. Menchaca-Rocha[71], E. Meninno[114,29], A.S. Menon[125], M. Meres[13],
S. Mhlanga[124,72], Y. Miake[134], L. Micheletti[59,24], L.C. Migliorin[136], D.L. Mihaylov[106],
K. Mikhaylov[75,93], A.N. Mishra[145], D. Miśkowiec[108], A. Modak[4], A.P. Mohanty[62],
B. Mohanty[87], M. Mohisin Khan[V,16], M.A. Molander[44], Z. Moravcova[90], C. Mordasini[106],
D.A. Moreira De Godoy[144], L.A.P. Moreno[45], I. Morozov[63], A. Morsch[34], T. Mrnjavac[34],
V. Muccifora[52], E. Mudnic[35], D. Mühlheim[144], S. Muhuri[141], J.D. Mulligan[80], A. Mulliri[22],
M.G. Munhoz[121], R.H. Munzer[68], H. Murakami[133], S. Murray[124], L. Musa[34], J. Musinsky[64],
J.W. Myrcha[142], B. Naik[132,49], R. Nair[86], B.K. Nandi[49], R. Nania[54], E. Nappi[53],
A.F. Nassirpour[81], A. Nath[105], C. Nattrass[131], A. Neagu[20], L. Nellen[69], S.V. Nesbo[36],
G. Neskovic[39], D. Nesterov[113], B.S. Nielsen[90], S. Nikolaev[89], S. Nikulin[89], V. Nikulin[99],
F. Noferini[54], S. Noh[12], P. Nomokonov[75], J. Norman[128], N. Novitzky[134], P. Nowakowski[142],
A. Nyanin[89], J. Nystrand[21], M. Ogino[83], A. Ohlson[81], V.A. Okorokov[94], J. Oleniacz[142],
A.C. Oliveira Da Silva[131], M.H. Oliver[146], A. Onnerstad[126], C. Oppedisano[59],
A. Ortiz Velasquez[69], T. Osako[46], A. Oskarsson[81], J. Otwinowski[118], M. Oya[46],
K. Oyama[83], Y. Pachmayer[105], S. Padhan[49], D. Pagano[140,58], G. Paić[69], A. Palasciano[53],
J. Pan[143], S. Panebianco[138], P. Pareek[141], J. Park[61], J.E. Parkkila[126], S.P. Pathak[125],
R.N. Patra[102,34], B. Paul[22], H. Pei[7], T. Peitzmann[62], X. Peng[7], L.G. Pereira[70],
H. Pereira Da Costa[138], D. Peresunko[89,82], G.M. Perez[8], S. Perrin[138], Y. Pestov[5],
V. Petráček[37], M. Petrovici[48], R.P. Pezzi[115,70], S. Piano[60], M. Pikna[13], P. Pillot[115],
O. Pinazza[54,34], L. Pinsky[125], C. Pinto[26], S. Pisano[52], M. Płoskoń[80], M. Planinic[100],
F. Pliquett[68], M.G. Poghosyan[97], B. Polichtchouk[92], S. Politano[30], N. Poljak[100], A. Pop[48],

S. Porteboeuf-Houssais[135], J. Porter[80], V. Pozdniakov[75], S.K. Prasad[4], R. Preghenella[54],
F. Prino[59], C.A. Pruneau[143], I. Pshenichnov[63], M. Puccio[34], S. Qiu[91], L. Quaglia[24],
R.E. Quishpe[125], S. Ragoni[111], A. Rakotozafindrabe[138], L. Ramello[31], F. Rami[137],
S.A.R. Ramirez[45], A.G.T. Ramos[33], T.A. Rancien[79], R. Raniwala[103], S. Raniwala[103],
S.S. Räsänen[44], R. Rath[50], I. Ravasenga[91], K.F. Read[97,131], A.R. Redelbach[39],
K. Redlich[VI,86], A. Rehman[21], P. Reichelt[68], F. Reidt[34], H.A. Reme-ness[36], R. Renfordt[68],
Z. Rescakova[38], K. Reygers[105], A. Riabov[99], V. Riabov[99], T. Richert[81], M. Richter[20],
W. Riegler[34], F. Riggi[26], C. Ristea[67], M. Rodríguez Cahuantzi[45], K. Røed[20], R. Rogalev[92],
E. Rogochaya[75], T.S. Rogoschinski[68], D. Rohr[34], D. Röhrich[21], P.F. Rojas[45],
P.S. Rokita[142], F. Ronchetti[52], A. Rosano[32,56], E.D. Rosas[69], A. Rossi[57], A. Rotondi[28,58],
A. Roy[50], P. Roy[110], S. Roy[49], N. Rubini[25], O.V. Rueda[81], R. Rui[23], B. Rumyantsev[75],
P.G. Russek[2], A. Rustamov[88], E. Ryabinkin[89], Y. Ryabov[99], A. Rybicki[118],
H. Rytkonen[126], W. Rzesa[142], O.A.M. Saarimaki[44], R. Sadek[115], S. Sadovsky[92], J. Saetre[21],
K. Šafařík[37], S.K. Saha[141], S. Saha[87], B. Sahoo[49], P. Sahoo[49], R. Sahoo[50], S. Sahoo[65],
D. Sahu[50], P.K. Sahu[65], J. Saini[141], S. Sakai[134], S. Sambyal[102], V. Samsonov[I,99,94],
D. Sarkar[143], N. Sarkar[141], P. Sarma[42], V.M. Sarti[106], M.H.P. Sas[146], J. Schambach[97,119],
H.S. Scheid[68], C. Schiaua[48], R. Schicker[105], A. Schmah[105], C. Schmidt[108], H.R. Schmidt[104],
M.O. Schmidt[34], M. Schmidt[104], N.V. Schmidt[97,68], A.R. Schmier[131], R. Schotter[137],
J. Schukraft[34], Y. Schutz[137], K. Schwarz[108], K. Schweda[108], G. Scioli[25], E. Scomparin[59],
J.E. Seger[15], Y. Sekiguchi[133], D. Sekihata[133], I. Selyuzhenkov[108,94], S. Senyukov[137],
J.J. Seo[61], D. Serebryakov[63], L. Šerkšnytė[106], A. Sevcenco[67], T.J. Shaba[72], A. Shabanov[63],
A. Shabetai[115], R. Shahoyan[34], W. Shaikh[110], A. Shangaraev[92], A. Sharma[101],
H. Sharma[118], M. Sharma[102], N. Sharma[101], S. Sharma[102], U. Sharma[102], O. Sheibani[125],
K. Shigaki[46], M. Shimomura[84], S. Shirinkin[93], Q. Shou[40], Y. Sibiriak[89], S. Siddhanta[55],
T. Siemiarczuk[86], T.F. Silva[121], D. Silvermyr[81], G. Simonetti[34], B. Singh[106], R. Singh[87],
R. Singh[102], R. Singh[50], V.K. Singh[141], V. Singhal[141], T. Sinha[110], B. Sitar[13], M. Sitta[31],
T.B. Skaali[20], G. Skorodumovs[105], M. Slupecki[44], N. Smirnov[146], R.J.M. Snellings[62],
C. Soncco[112], J. Song[125], A. Songmoolnak[116], F. Soramel[27], S. Sorensen[131],
I. Sputowska[118], J. Stachel[105], I. Stan[67], P.J. Steffanic[131], S.F. Stiefelmaier[105], D. Stocco[115],
I. Storehaug[20], M.M. Storetvedt[36], C.P. Stylianidis[91], A.A.P. Suaide[121], T. Sugitate[46],
C. Suire[78], M. Sukhanov[63], M. Suljic[34], R. Sultanov[93], M. Šumbera[96], V. Sumberia[102],
S. Sumowidagdo[51], S. Swain[65], A. Szabo[13], I. Szarka[13], U. Tabassam[14], S.F. Taghavi[106],
G. Taillepied[135], J. Takahashi[122], G.J. Tambave[21], S. Tang[135,7], Z. Tang[129],
J.D. Tapia Takaki[VII,127], M. Tarhini[115], M.G. Tarzila[48], A. Tauro[34], G. Tejeda Muñoz[45],
A. Telesca[34], L. Terlizzi[24], C. Terrevoli[125], G. Tersimonov[3], S. Thakur[141], D. Thomas[119],
R. Tieulent[136], A. Tikhonov[63], A.R. Timmins[125], M. Tkacik[117], A. Toia[68], N. Topilskaya[63],
M. Toppi[52], F. Torales-Acosta[19], T. Tork[78], S.R. Torres[37], A. Trifiró[32,56], S. Tripathy[54,69],
T. Tripathy[49], S. Trogolo[34,27], G. Trombetta[33], V. Trubnikov[3], W.H. Trzaska[126],
T.P. Trzcinski[142], B.A. Trzeciak[37], A. Tumkin[109], R. Turrisi[57], T.S. Tveter[20],
K. Ullaland[21], A. Uras[136], M. Urioni[58,140], G.L. Usai[22], M. Vala[38], N. Valle[58,28],
S. Vallero[59], N. van der Kolk[62], L.V.R. van Doremalen[62], M. van Leeuwen[91],
P. Vande Vyvre[34], D. Varga[145], Z. Varga[145], M. Varga-Kofarago[145], A. Vargas[45],
M. Vasileiou[85], A. Vasiliev[89], O. Vázquez Doce[52,106], V. Vechernin[113], E. Vercellin[24],

S. Vergara Limón[45], L. Vermunt[62], R. Vértesi[145], M. Verweij[62], L. Vickovic[35],
Z. Vilakazi[132], O. Villalobos Baillie[111], G. Vino[53], A. Vinogradov[89], T. Virgili[29],
V. Vislavicius[90], A. Vodopyanov[75], B. Volkel[34], M.A. Völkl[105], K. Voloshin[93],
S.A. Voloshin[143], G. Volpe[33], B. von Haller[34], I. Vorobyev[106], D. Voscek[117], N. Vozniuk[63],
J. Vrláková[38], B. Wagner[21], C. Wang[40], D. Wang[40], M. Weber[114], R.J.G.V. Weelden[91],
A. Wegrzynek[34], S.C. Wenzel[34], J.P. Wessels[144], J. Wiechula[68], J. Wikne[20], G. Wilk[86],
J. Wilkinson[108], G.A. Willems[144], B. Windelband[105], M. Winn[138], W.E. Witt[131],
J.R. Wright[119], W. Wu[40], Y. Wu[129], R. Xu[7], A.K. Yadav[141], S. Yalcin[77], Y. Yamaguchi[46],
K. Yamakawa[46], S. Yang[21], S. Yano[46], Z. Yin[7], H. Yokoyama[62], I.-K. Yoo[17], J.H. Yoon[61],
S. Yuan[21], A. Yuncu[105], V. Zaccolo[23], C. Zampolli[34], H.J.C. Zanoli[62], N. Zardoshti[34],
A. Zarochentsev[113], P. Závada[66], N. Zaviyalov[109], M. Zhalov[99], B. Zhang[7], S. Zhang[40],
X. Zhang[7], Y. Zhang[129], V. Zherebchevskii[113], Y. Zhi[11], N. Zhigareva[93], D. Zhou[7],
Y. Zhou[90], J. Zhu[7,108], Y. Zhu[7], A. Zichichi[25], G. Zinovjev[3], N. Zurlo[140,58]

1   A.I. Alikhanyan National Science Laboratory (Yerevan Physics Institute) Foundation,
    Yerevan, Armenia
2   AGH University of Science and Technology, Cracow, Poland
3   Bogolyubov Institute for Theoretical Physics, National Academy of Sciences of Ukraine, Kiev, Ukraine
4   Bose Institute, Department of Physics and Centre for Astroparticle Physics and Space Science
    (CAPSS), Kolkata, India
5   Budker Institute for Nuclear Physics, Novosibirsk, Russia
6   California Polytechnic State University, San Luis Obispo, California, United States
7   Central China Normal University, Wuhan, China
8   Centro de Aplicaciones Tecnológicas y Desarrollo Nuclear (CEADEN), Havana, Cuba
9   Centro de Investigación y de Estudios Avanzados (CINVESTAV), Mexico City and Mérida, Mexico
10 Chicago State University, Chicago, Illinois, United States
11 China Institute of Atomic Energy, Beijing, China
12 Chungbuk National University, Cheongju, Republic of Korea
13 Comenius University Bratislava, Faculty of Mathematics, Physics and Informatics,
    Bratislava, Slovakia
14 COMSATS University Islamabad, Islamabad, Pakistan
15 Creighton University, Omaha, Nebraska, United States
16 Department of Physics, Aligarh Muslim University, Aligarh, India
17 Department of Physics, Pusan National University, Pusan, Republic of Korea
18 Department of Physics, Sejong University, Seoul, Republic of Korea
19 Department of Physics, University of California, Berkeley, California, United States
20 Department of Physics, University of Oslo, Oslo, Norway
21 Department of Physics and Technology, University of Bergen, Bergen, Norway
22 Dipartimento di Fisica dell'Università and Sezione INFN, Cagliari, Italy
23 Dipartimento di Fisica dell'Università and Sezione INFN, Trieste, Italy
24 Dipartimento di Fisica dell'Università and Sezione INFN, Turin, Italy
25 Dipartimento di Fisica e Astronomia dell'Università and Sezione INFN, Bologna, Italy
26 Dipartimento di Fisica e Astronomia dell'Università and Sezione INFN, Catania, Italy
27 Dipartimento di Fisica e Astronomia dell'Università and Sezione INFN, Padova, Italy
28 Dipartimento di Fisica e Nucleare e Teorica, Università di Pavia, Pavia, Italy
29 Dipartimento di Fisica 'E.R. Caianiello' dell'Università and Gruppo Collegato INFN, Salerno, Italy
30 Dipartimento DISAT del Politecnico and Sezione INFN, Turin, Italy
31 Dipartimento di Scienze e Innovazione Tecnologica dell'Università del Piemonte Orientale and INFN
    Sezione di Torino, Alessandria, Italy

[32] *Dipartimento di Scienze MIFT, Università di Messina, Messina, Italy*

[33] *Dipartimento Interateneo di Fisica 'M. Merlin' and Sezione INFN, Bari, Italy*

[34] *European Organization for Nuclear Research (CERN), Geneva, Switzerland*

[35] *Faculty of Electrical Engineering, Mechanical Engineering and Naval Architecture, University of Split, Split, Croatia*

[36] *Faculty of Engineering and Science, Western Norway University of Applied Sciences, Bergen, Norway*

[37] *Faculty of Nuclear Sciences and Physical Engineering, Czech Technical University in Prague, Prague, Czech Republic*

[38] *Faculty of Science, P.J. Šafárik University, Košice, Slovakia*

[39] *Frankfurt Institute for Advanced Studies, Johann Wolfgang Goethe-Universität Frankfurt, Frankfurt, Germany*

[40] *Fudan University, Shanghai, China*

[41] *Gangneung-Wonju National University, Gangneung, Republic of Korea*

[42] *Gauhati University, Department of Physics, Guwahati, India*

[43] *Helmholtz-Institut für Strahlen- und Kernphysik, Rheinische Friedrich-Wilhelms-Universität Bonn, Bonn, Germany*

[44] *Helsinki Institute of Physics (HIP), Helsinki, Finland*

[45] *High Energy Physics Group, Universidad Autónoma de Puebla, Puebla, Mexico*

[46] *Hiroshima University, Hiroshima, Japan*

[47] *Hochschule Worms, Zentrum für Technologietransfer und Telekommunikation (ZTT), Worms, Germany*

[48] *Horia Hulubei National Institute of Physics and Nuclear Engineering, Bucharest, Romania*

[49] *Indian Institute of Technology Bombay (IIT), Mumbai, India*

[50] *Indian Institute of Technology Indore, Indore, India*

[51] *Indonesian Institute of Sciences, Jakarta, Indonesia*

[52] *INFN, Laboratori Nazionali di Frascati, Frascati, Italy*

[53] *INFN, Sezione di Bari, Bari, Italy*

[54] *INFN, Sezione di Bologna, Bologna, Italy*

[55] *INFN, Sezione di Cagliari, Cagliari, Italy*

[56] *INFN, Sezione di Catania, Catania, Italy*

[57] *INFN, Sezione di Padova, Padova, Italy*

[58] *INFN, Sezione di Pavia, Pavia, Italy*

[59] *INFN, Sezione di Torino, Turin, Italy*

[60] *INFN, Sezione di Trieste, Trieste, Italy*

[61] *Inha University, Incheon, Republic of Korea*

[62] *Institute for Gravitational and Subatomic Physics (GRASP), Utrecht University/Nikhef, Utrecht, Netherlands*

[63] *Institute for Nuclear Research, Academy of Sciences, Moscow, Russia*

[64] *Institute of Experimental Physics, Slovak Academy of Sciences, Košice, Slovakia*

[65] *Institute of Physics, Homi Bhabha National Institute, Bhubaneswar, India*

[66] *Institute of Physics of the Czech Academy of Sciences, Prague, Czech Republic*

[67] *Institute of Space Science (ISS), Bucharest, Romania*

[68] *Institut für Kernphysik, Johann Wolfgang Goethe-Universität Frankfurt, Frankfurt, Germany*

[69] *Instituto de Ciencias Nucleares, Universidad Nacional Autónoma de México, Mexico City, Mexico*

[70] *Instituto de Física, Universidade Federal do Rio Grande do Sul (UFRGS), Porto Alegre, Brazil*

[71] *Instituto de Física, Universidad Nacional Autónoma de México, Mexico City, Mexico*

[72] *iThemba LABS, National Research Foundation, Somerset West, South Africa*

[73] *Jeonbuk National University, Jeonju, Republic of Korea*

[74] *Johann-Wolfgang-Goethe Universität Frankfurt Institut für Informatik, Fachbereich Informatik und Mathematik, Frankfurt, Germany*

[75] *Joint Institute for Nuclear Research (JINR), Dubna, Russia*

[76] *Korea Institute of Science and Technology Information, Daejeon, Republic of Korea*

77 *KTO Karatay University, Konya, Turkey*

78 *Laboratoire de Physique des 2 Infinis, Irène Joliot-Curie, Orsay, France*

79 *Laboratoire de Physique Subatomique et de Cosmologie, Université Grenoble-Alpes, CNRS-IN2P3, Grenoble, France*

80 *Lawrence Berkeley National Laboratory, Berkeley, California, United States*

81 *Lund University Department of Physics, Division of Particle Physics, Lund, Sweden*

82 *Moscow Institute for Physics and Technology, Moscow, Russia*

83 *Nagasaki Institute of Applied Science, Nagasaki, Japan*

84 *Nara Women's University (NWU), Nara, Japan*

85 *National and Kapodistrian University of Athens, School of Science, Department of Physics, Athens, Greece*

86 *National Centre for Nuclear Research, Warsaw, Poland*

87 *National Institute of Science Education and Research, Homi Bhabha National Institute, Jatni, India*

88 *National Nuclear Research Center, Baku, Azerbaijan*

89 *National Research Centre Kurchatov Institute, Moscow, Russia*

90 *Niels Bohr Institute, University of Copenhagen, Copenhagen, Denmark*

91 *Nikhef, National institute for subatomic physics, Amsterdam, Netherlands*

92 *NRC Kurchatov Institute IHEP, Protvino, Russia*

93 *NRC «Kurchatov»Institute — ITEP, Moscow, Russia*

94 *NRNU Moscow Engineering Physics Institute, Moscow, Russia*

95 *Nuclear Physics Group, STFC Daresbury Laboratory, Daresbury, United Kingdom*

96 *Nuclear Physics Institute of the Czech Academy of Sciences, Řež u Prahy, Czech Republic*

97 *Oak Ridge National Laboratory, Oak Ridge, Tennessee, United States*

98 *Ohio State University, Columbus, Ohio, United States*

99 *Petersburg Nuclear Physics Institute, Gatchina, Russia*

100 *Physics department, Faculty of science, University of Zagreb, Zagreb, Croatia*

101 *Physics Department, Panjab University, Chandigarh, India*

102 *Physics Department, University of Jammu, Jammu, India*

103 *Physics Department, University of Rajasthan, Jaipur, India*

104 *Physikalisches Institut, Eberhard-Karls-Universität Tübingen, Tübingen, Germany*

105 *Physikalisches Institut, Ruprecht-Karls-Universität Heidelberg, Heidelberg, Germany*

106 *Physik Department, Technische Universität München, Munich, Germany*

107 *Politecnico di Bari and Sezione INFN, Bari, Italy*

108 *Research Division and ExtreMe Matter Institute EMMI, GSI Helmholtzzentrum für Schwerionenforschung GmbH, Darmstadt, Germany*

109 *Russian Federal Nuclear Center (VNIIEF), Sarov, Russia*

110 *Saha Institute of Nuclear Physics, Homi Bhabha National Institute, Kolkata, India*

111 *School of Physics and Astronomy, University of Birmingham, Birmingham, United Kingdom*

112 *Sección Física, Departamento de Ciencias, Pontificia Universidad Católica del Perú, Lima, Peru*

113 *St. Petersburg State University, St. Petersburg, Russia*

114 *Stefan Meyer Institut für Subatomare Physik (SMI), Vienna, Austria*

115 *SUBATECH, IMT Atlantique, Université de Nantes, CNRS-IN2P3, Nantes, France*

116 *Suranaree University of Technology, Nakhon Ratchasima, Thailand*

117 *Technical University of Košice, Košice, Slovakia*

118 *The Henryk Niewodniczanski Institute of Nuclear Physics, Polish Academy of Sciences, Cracow, Poland*

119 *The University of Texas at Austin, Austin, Texas, United States*

120 *Universidad Autónoma de Sinaloa, Culiacán, Mexico*

121 *Universidade de São Paulo (USP), São Paulo, Brazil*

122 *Universidade Estadual de Campinas (UNICAMP), Campinas, Brazil*

123 *Universidade Federal do ABC, Santo Andre, Brazil*

124 *University of Cape Town, Cape Town, South Africa*

125 University of Houston, Houston, Texas, United States
126 University of Jyväskylä, Jyväskylä, Finland
127 University of Kansas, Lawrence, Kansas, United States
128 University of Liverpool, Liverpool, United Kingdom
129 University of Science and Technology of China, Hefei, China
130 University of South-Eastern Norway, Tonsberg, Norway
131 University of Tennessee, Knoxville, Tennessee, United States
132 University of the Witwatersrand, Johannesburg, South Africa
133 University of Tokyo, Tokyo, Japan
134 University of Tsukuba, Tsukuba, Japan
135 Université Clermont Auvergne, CNRS/IN2P3, LPC, Clermont-Ferrand, France
136 Université de Lyon, CNRS/IN2P3, Institut de Physique des 2 Infinis de Lyon, Lyon, France
137 Université de Strasbourg, CNRS, IPHC UMR 7178, F-67000 Strasbourg, France, Strasbourg, France
138 Université Paris-Saclay Centre d'Etudes de Saclay (CEA), IRFU, Départment de Physique Nucléaire (DPhN), Saclay, France
139 Università degli Studi di Foggia, Foggia, Italy
140 Università di Brescia, Brescia, Italy
141 Variable Energy Cyclotron Centre, Homi Bhabha National Institute, Kolkata, India
142 Warsaw University of Technology, Warsaw, Poland
143 Wayne State University, Detroit, Michigan, United States
144 Westfälische Wilhelms-Universität Münster, Institut für Kernphysik, Münster, Germany
145 Wigner Research Centre for Physics, Budapest, Hungary
146 Yale University, New Haven, Connecticut, United States
147 Yonsei University, Seoul, Republic of Korea

I Deceased
II Also at: Italian National Agency for New Technologies, Energy and Sustainable Economic Development (ENEA), Bologna, Italy
III Also at: Dipartimento DET del Politecnico di Torino, Turin, Italy
IV Also at: M.V. Lomonosov Moscow State University, D.V. Skobeltsyn Institute of Nuclear, Physics, Moscow, Russia
V Also at: Department of Applied Physics, Aligarh Muslim University, Aligarh, India
VI Also at: Institute of Theoretical Physics, University of Wroclaw, Poland
VII Also at: University of Kansas, Lawrence, Kansas, United States